



HYPERFINE MAGNETIC FIELDS AT ^{181}Ta
IMPURITY NUCLEI IN FERROMAGNETIC ZrZn_2

HYPERFINE MAGNETIC FIELDS
AT ^{181}Tm IMPURITY NUCLEI
IN FERROMAGNETIC ZrZn_2

By

JOHN STEPHEN BARRETT, B.Sc.

A Thesis

Submitted to the Faculty of Graduate Studies
in Partial Fulfillment of the Requirements
for the Degree
Doctor of Philosophy

McMaster University

September 1974

© JOHN STEPHEN BARRETT 1975

DOCTOR OF PHILOSOPHY
(Physics)

McMASTER UNIVERSITY
Hamilton, Ontario.

TITLE: Hyperfine Magnetic Fields at ^{181}Ta Impurity
Nuclei in Ferromagnetic ZrZn_2

AUTHOR: John Stephen Barrett, B.Sc. (McMaster University)

SUPERVISOR: Professor J. A. Cameron

NUMBER OF PAGES: viii, 89

SCOPE AND CONTENTS:

The hyperfine magnetic field at ^{181}Ta nuclei substituting at the zirconium sites in ferromagnetic ZrZn_2 was measured by the method of time-differential perturbed angular correlations (TDPAC). The value obtained was -17.3 ± 0.3 kOe with 2% hafnium impurity at the zirconium sites.

The hyperfine field was also measured as a function of hafnium and titanium concentration (substituting at zirconium sites) and compared with magnetization measurements on the same samples. The magnetization data agreed qualitatively with measurements by Ogawa: the magnetization decreases to zero at about 15% hafnium concentration, but increases to a maximum at about 20% titanium concentration. The hyperfine field, however, decreases less rapidly with hafnium concentration but drops off fairly suddenly near 20% hafnium. When titanium impurity is added, the hyperfine field does not increase by as great a fraction as does the magnetization.

ACKNOWLEDGEMENTS

First and especially, I would like to thank my supervisor, Dr. J. A. Cameron for all his help and good advice. His encouragement and sense of humour were also much appreciated.

I wish to extend my thanks to the others who have contributed to this work:

To the members of my advisory committee - Dr. M. P. Collins and Dr. T. Birchall.

To Dr. W. Smeltzer, the first one I consulted about making $ZrZn_2$ who didn't say, "Why on earth do you want to make that?"

To Dr. D. W. Taylor for helpful discussions about band model calculations.

To Jim O'Donnell for making the ingots from which the samples were made.

To Dr. C. W. Stager for the use of his vibrating sample magnetometer, and to John Niemans who did all the hard work involved with making the bulk magnetization measurements.

To Aquila Islam and Terry Taylor who shared my plight in the dreary dungeon of the nuclear research building and made it endurable.

To Dr. S. Wender for his help with experiments.

To Leo Love for helpful discussions about experimental techniques.

To Mr. R. McNaught, who designed and built the interface for the PDP 11/05 computer and helped me learn to program it.

To Mr. H. Blanchard, who repaired the electronics when things stopped working.

I would also like to express my appreciation to Dr. S. Ogawa, for his prompt and very helpful replies to my questions about $ZrZn_2$.

I want to thank my mother, who typed this thesis and is still not my enemy; my wife Sharon, for her patience and encouragement - and last of all, my thanks to Adrienne who helped me write the thesis.

To Sharon

TABLE OF CONTENTS

	Page
I INTRODUCTION	1
II MAGNETISM AND HYPERFINE FIELDS IN METALS	
1. MODELS FOR FERROMAGNETISM IN METALS	12
2. ORDERING OF MAGNETIC MOMENTS	14
3. THE STONER MODEL AND ITS APPLICATION TO FERROMAGNETIC $ZrZn_2$	15
4. THE SINGLE IMPURITY	19
5. HYPERFINE FIELDS	
(a) Magnetic fields	20
(b) Electric field gradients	22
III γ - γ ANGULAR CORRELATIONS	
1. UNPERTURBED ANGULAR CORRELATION	25
2. PERTURBED ANGULAR CORRELATIONS	
(a) Magnetic fields	26
(b) Electric field gradients	29
(c) Time dependent perturbations	30
3. TIME RESOLUTION	31
IV EXPERIMENTAL ARRANGEMENT	
1. THE APPARATUS	
(a) Scintillators, photomultiplier tubes and tube bases	32
(b) Discriminators	34

	Page
2. TIME CALIBRATION	35
3. NON-LINEARITY	35
4. THE MAGNET	37
5. THE DEMAGNETIZING FACTOR	41
V SAMPLE PREPARATION AND ANALYSIS	
1. SAMPLE REPRODUCIBILITY	42
2. SAMPLE PREPARATION	44
3. NEUTRON ACTIVATION ANALYSIS	46
4. X-RAY ANALYSIS	48
5. BULK MAGNETIZATION MEASUREMENTS	50
6. CORRECTION TO THE MAGNETIZATION	50
VI DATA ANALYSIS AND EXPERIMENTAL RESULTS	
1. DATA ANALYSIS	57
2. BACKGROUND SUBTRACTION	62
3. STATISTICAL ERROR	63
4. EXPERIMENTAL RESULTS	65
VII DISCUSSION OF THE RESULTS AND INTERPRETATION	
1. THE AMPLITUDE OF THE OSCILLATIONS	70
2. ZINC CONCENTRATION IN THE $ZrZn_2$ SAMPLES	71
3. THE MAGNITUDE AND SIGN OF THE HYPERFINE FIELD	73
4. IMPURITY CONCENTRATION DEPENDENCE OF THE HYPERFINE FIELD	75
APPENDIX PROGRAM DIFCOR	78
REFERENCES	87

LIST OF FIGURES

		Page
I-1	Unit cell of $ZrZn_2$	6
II-1	Point symmetry about Ta impurity atom	24
III-1	Level scheme of ^{181}Ta	28
IV-1	Schematic diagram of the apparatus	33
IV-2	Differential non-linearity curve	36
IV-3	Time spectrum for the decay of the 482-keV state in ^{181}Ta	38
IV-4	Calculated magnetic field inhomogeneity for the magnet used in the hyperfine field measurements	40
V-1	Phase diagram for zirconium-zinc	43
V-2	A portion of the powder X-ray spectrum	49
V-3	The measured bulk magnetization as a function of field for samples 8, 1 and 10	51
V-4	The measured bulk magnetization as a function of field for samples 14, 11, 4, 7, 12 and 5	52
V-5	$M^2(0,T)$ plotted against T^2 for samples 8, 10 and 1	53
V-6	$M^2(0,T)$ plotted against T^2 for samples 14 and 11	54
VI-1	Detector configuration and angular correlation patterns	58
VI-2	An example of the untreated data	59
VI-3	The function $R(t)$ and least squares fit for sample 8 at 300°K and 4°K	61

	Page	
VI-4	The function $R(t)$ and least squares fit. for samples 1, 10, 4, 12, 5, 7, 11 and 14 at 4°K	66
VI-5	The hyperfine field and bulk magnetization plotted as a function of hafnium and titanium concentrations	68
VII-1	The conduction electron polarization (CEP) model for the hyperfine field at Ta in 3d ferromagnets	76

LIST OF TABLES

	Page
V-1 Summary of sample preparations and zinc concentrations	47
V-2 Magnetic fraction of the samples	56
VI-1 Bulk magnetizations and hyperfine fields	67

CHAPTER I

INTRODUCTION

Magnetism is a phenomenon which has always held a strong fascination for people. Although an immense amount has been learned about it, there are still simple questions (like "why is one material magnetic and another not?") which do not have simple answers. This will likely always be so. The reason is that the presence of magnetism depends on the complicated electronic structures of the atoms and also on the arrangement of the atoms in the particular material. The atoms do not behave individually but, because of their close proximity, interact with one another. Some of their electrons are shared to a large extent with all the other atoms, and even those which are not shared have a different behaviour from what it would be for a single free atom.

The origin of the magnetism itself is with the electrons. An electromagnet is made by passing a current through a coil of wire. Likewise, in a magnetic substance, the magnetism can come from the circulation of electrons about the atomic nuclei (orbital angular momentum). Besides this, every electron has some intrinsic magnetism which may be thought of as originating from the electron's spinning on its axis (spin angular momentum). The electrons are like tiny identical magnets, each having a magnetic moment of one Bohr magneton: μ_B . A magnetic moment μ can be defined by the energy E and

the torque $\vec{\tau}$ for a magnet in a magnetic field \vec{H} . The equations are:

$$\vec{E} = -\vec{\mu} \cdot \vec{H} \quad (I-1)$$

and
$$\vec{\tau} = \vec{\mu} \times \vec{H} \quad (I-2)$$

The spins of the electrons may be oriented in one of two ways with respect to some arbitrary direction: either parallel or anti-parallel. They are usually called "spin up" or "spin down" electrons.

The materials described in this thesis are crystals, which means that the atoms are arranged in an orderly array or lattice. There may be unpaired spins between the atoms in the lattice or right at the atoms, in which case a local moment is said to have formed. The orbital angular momentum also contributes to this moment. Usually, but not always, these moments will be the same size at all atoms of the same kind in the crystal. In ferromagnets, these moments align in the same direction within small regions called domains. This ordering occurs only below a critical temperature called the Curie temperature: T_c . As the temperature increases towards T_c , the orientations of the moments within a domain fluctuate more and more, so that the moment per unit volume of the domain (called the saturation magnetization) decreases. The total moments of the domains need not be aligned and this is why iron for instance is not always magnetized. As large magnetic fields are applied, the domains align and the saturation magnetization is approached by the magnetization of the whole sample. Above the Curie temperature the magnetization is not spontaneous but it can be induced by applying a magnetic field. This is called para-

magnetism. The bulk magnetization for a sample can be measured in field-intensity per unit volume or unit weight. The practice followed in this thesis is to use the bulk moment which is the number of Bohr magnetons per atom of zirconium.

From the previous discussion it can be seen that magnetism can be considered on different scales of size. The types of measurements that can be made fall naturally into two categories: macroscopic and microscopic. Much can be learned about the magnetism of a material from bulk magnetization measurements at different temperatures and applied fields. This is a macroscopic measurement. The unpaired spin density (a microscopic property) can be measured throughout the lattice by diffuse scattering of neutrons. The particular contribution of this thesis involves the measurement of magnetic fields at an atomic nucleus in a ferromagnet. The field at the nucleus is called the hyperfine magnetic field.

The best theoretical approach to describe magnetic materials varies. In the "rare earth" elements, the electrons responsible for magnetism are well localized and the orbital angular momentum plays an important role. The "transition series" elements are the intermediate case: the degree of localization is much less and the electron spin provides the dominant contribution to the magnetism.

The opposite extreme to a ferromagnet having localized moments is one in which the electrons responsible for the magnetism are itinerant. In 1938, Stoner proposed a band model to describe this kind of ferromagnet. In single free atoms, the electrons have

discrete energies but in a crystal, because of the interaction of the atoms, their outer electrons can have a continuous "band" of energies within a certain range called the band-width. The number of electrons with a specified energy in a band is called the density of states for that energy. In Stoner's model, there is a band of spin up d electrons (a kind of electron having a particular orbital angular momentum in the atom) and a band of spin down d electrons. The bands have electrons up to a fairly sharp cutoff in energy called the Fermi level. If the material were not magnetic, the two bands would be at identical energies but, because of interactions between the "up" and the "down" electrons, the bands shift - one upwards in energy, the other downwards. The amount is called the band splitting. Because of the definite energy cutoff at the Fermi level, the electrons from the band that moves upward are removed and added to the band that moves downward. There are then more electrons of one spin than of the other and the material is magnetic.

Before the relatively recent discovery of $ZrZn_2$ there was no existing ferromagnet to which the theory suitably applied (the theory for a very weak itinerant ferromagnet).

A lively interest has arisen in this alloy of zirconium and zinc (neither of which is magnetic) because its magnetic properties are different from those of typical ferromagnets. $ZrZn_2$ was first reported to be a ferromagnet by Matthias and Bozorth in 1958. It has a Curie temperature of about 26K and a saturation moment around $0.16 \mu_B$ per zirconium site.

Foner et al. in 1967 suggested that the ferromagnetism was induced by impurities and that $ZrZn_2$ might not be intrinsically ferromagnetic. Ogawa and also Blythe, however, have made magnetic samples with less than 100 ppm transition impurity.

Using Stoner's band model for a very weak itinerant ferromagnet (see Section II-3), Wohlfarth has deduced that the band splitting is about 0.04 eV and the density of states at the Fermi surface is 2.9 states/atom/eV. Band structure calculations for the cubic Laves structure (Fig. I-1) ($MgCu_2$ type) by Koelling et al. (KJK!) have resulted in a splitting of approximately half that amount since the calculated density of states is about twice Wohlfarth's value. The width of the band is calculated to be about 0.2 eV.

Shirane et al., using magnetic neutron scattering, showed that the unpaired spin density is associated with the zirconium sites rather than the zinc and that there is a maximum in the density midway between zirconium sites.

Measurements of the magnetization of $ZrZn_2$ with hafnium and titanium impurities by Ogawa provided the motivation for the experiments in this thesis. The magnetization decreased to zero when about 15% of the zirconium atoms were replaced with hafnium, but the magnetization increased to a maximum at 20% titanium.

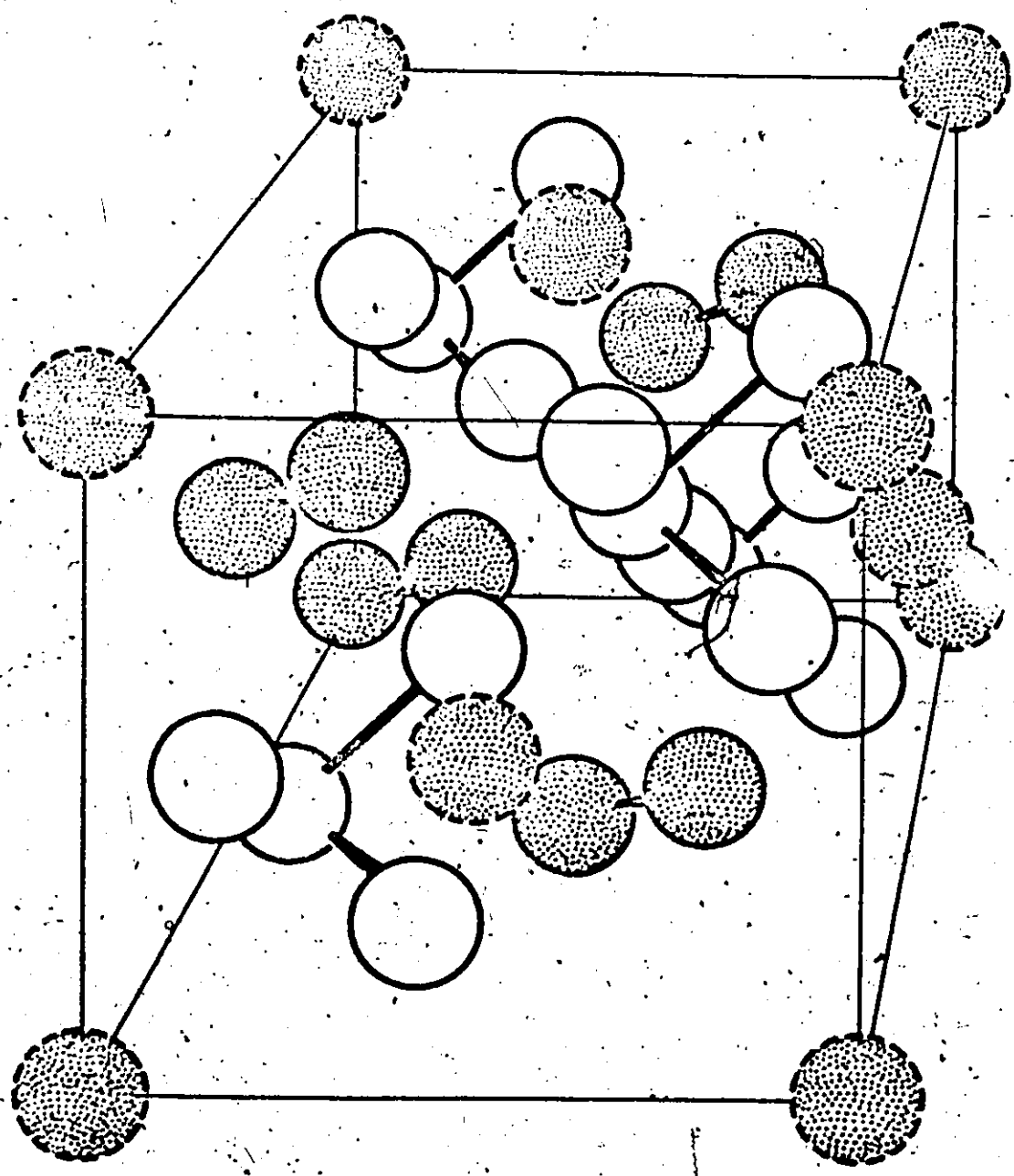
Murdóch et al. were able to fix an upper limit of 22 kOe for the magnitude of the hyperfine field at ^{97}Nb in $ZrZn_2$, using nuclear orientation. Time-differential perturbed angular correlations (TDPAC) offered the possibility of measuring lower hyperfine fields at ^{181}Ta nuclei.

Figure I-1

Unit Cell of $ZrZn_2$

The dark circles represent zirconium atoms.

The open circles arranged in tetrahedra represent
the zinc atoms.



3

formed in the decay of radioactive ^{181}Hf . Hafnium would be expected to occupy zirconium sites since the metals are very similar and natural zirconium contains a few percent hafnium.

The method of time-differential perturbed angular correlations will now be briefly described.

The radioactive nucleus ^{181}Hf decays to ^{181}Ta with the emission of two successive gamma rays which can be distinguished by their energies. The nucleus can be pictured as spinning on its axis. The probability of emission of a gamma ray from the nucleus has an anisotropic distribution which depends on the orientations of the nucleus before and after emission. Because the nucleus has a random orientation, the first gamma ray γ_1 has an equal probability of being detected in any direction. Once it is detected, however, the nuclear axis has a preferred orientation so that the probability distribution of the second gamma ray γ_2 is anisotropic. This distribution is called the angular correlation.

A torque is produced on a nucleus having a magnetic dipole moment when a magnetic field is applied. The nucleus then undergoes classical Larmor precession about the field direction like a spinning top in a gravitational field. In both cases (at least to a good approximation for a top with a heavy rim) the rate of precession is proportional to the field strength but independent of orientation. Because this is so, the angular correlation rotates about the field direction and retains its shape. It is now called a perturbed angular correlation.

The term "time-differential" refers to the method of observing the perturbed angular correlation. For each γ_1 detected, if a γ_2 is also detected by another fixed counter, the time between the two gamma rays is measured. The number of γ_2 s plotted against this time interval decreases exponentially but there is also a periodic modulation of the intensity because of the rotation of the angular correlation pattern (Fig. VI-1 and VI-2). The frequency of this oscillation is double the precession frequency (Eqn. III-2) because there are two maxima and minima for each rotation of the pattern.

Chapter II discusses different models of ferromagnetism with stress on Stoner theory which is used in Chapter V for the analysis of bulk magnetization data for $ZrZn_2$. Chapter II also discusses magnetic and electric interactions with the nucleus (hyperfine fields).

Chapter III describes the effect of magnetic and electric perturbations on the correlation pattern, giving examples for ^{181}Tm under different experimental conditions.

Chapter IV concerns the apparatus used: calibration of the electronics and the size and homogeneity of the external magnetic field which was applied to samples during the hyperfine field measurements.

Chapter V is about the metallurgical condition of each sample. Its contents are crucial to the support of some of the conclusions drawn in this thesis. The method of sample preparation and the analyses by neutron activation and by X-ray diffraction are described. Also contained in this chapter are the bulk magnetization data and corrections to them because the samples contained some non-magnetic phase.

Chapter VI contains the results of the hyperfine field measurements. It demonstrates how the raw data are generated and how they are treated in order to analyze them. The hyperfine fields are compared with the bulk magnetization measurements.

Chapter VII summarizes the results and makes some attempt to explain them.

CHAPTER II

MAGNETISM AND HYPERFINE FIELDS IN METALS

A great deal can be understood about magnetism in the rare earth and transition series elements on the basis of a local moment model. Consequently, a large amount of research has been devoted to understanding how local moments form and how they interact with one another. The most important mechanism for their interaction is the polarization of the itinerant s electrons by the local moments. In order to understand this mechanism more fully, it is necessary to know the spatial distribution of the s electron spin polarization. The s electrons are the only electrons which have a large probability of existing at the atomic nucleus and at this particular location their net spin polarization can be measured by the resulting magnetic field at the nucleus. It is called the hyperfine magnetic field. There may be, however, another contribution to the hyperfine magnetic field and this is from the orbital angular momentum of all the other electrons.

In the rare earth elements, the orbital angular momentum of the $4f$ electrons provides the major contribution to the local magnetic moment and also contributes to the hyperfine field. The $3d$ electrons of iron, cobalt and nickel, though, are not as localized as this and are not well shielded from the intense electric fields from neighbouring atoms. This crystal field causes the Z component of the orbital angular momentum L_z to vary in time so that its average value is

small or zero. The orbital angular momentum is said to be "quenched" so that spin angular momentum predominates in the ferromagnetism of the iron group.

This thesis describes the measurement of hyperfine fields at UFe_2 . In this material, the electrons responsible for ferromagnetism are even less localized than those in elements of the iron group and the orbital angular momentum contribution is expected to be insignificant. In this case, the hyperfine magnetic field provides an unambiguous indication of the s electron spin polarization at the nucleus.

Probably the simplest picture of a magnetic material is one in which identical localized moments interact. In order to understand how these moments form and how they interact, one experimental technique is often employed: a single impurity atom is substituted for an atom in the pure material. For instance, the impurity atom may be one that is not from a magnetic metal and the host lattice may be a ferromagnet. Does a local moment form at the impurity? If one does, how big is it and how does it behave? How does it affect the host moments near it? Alternatively, a magnetic impurity can be put into a non-magnetic host and one may ask whether there is a moment, what its extent is, and whether it induces moments in the host. The aim is to learn about the behaviour of the local moments in the pure magnetic materials. The measurement of hyperfine fields at or near the single impurity is one of the experimental methods of obtaining some of this information.

The problem considered in this thesis is the behaviour of the hyperfine magnetic field at tantalum impurity nuclei substituting at the zirconium sites of ferromagnetic $ZrZn_2$. This material is well described in terms of a band model. The picture of interacting local moments previously mentioned does not apply because the electrons responsible for the magnetism are itinerant to a much greater degree. Do models predicting hyperfine fields in the iron group still apply? This is not an easy question to answer on theoretical grounds alone, and so the actual measurement contained in this thesis provides a guideline for applying and refining existing models or developing new ones if they are required.

The purpose of the rest of this chapter is to give more detail about some of the ideas already discussed. Both local moment models and band models have traditionally been applied to the iron group elements. Section 1 is a brief review of some of the developments that have taken place within the two approaches. The second section describes some of the predictions of the local moment model and Section 3 describes Stoner's band model and its application to $ZrZn_2$. Section 4 contains more considerations about single impurities. The last section is about hyperfine fields and their relation to magnetism.

1. MODELS FOR FERROMAGNETISM IN METALS

An excellent review of the development of models for ferromagnetism in metals has been written by Herring.

Since the 1930s there have been two models for magnetism and

this resulted in intense rivalry. The first is the Heisenberg model in which the moments are localized on the atomic sites and interact directly. It was successful in explaining the critical scattering of neutrons and in describing spin waves. It was Stoner who was mostly responsible for adapting band theory to magnetism. This is the other approach. It explains the fact that the d electrons responsible for ferromagnetism participate in conduction. It also explains why the magnetization at zero degrees need not be an integral number of Bohr magnetons per atom. A simple band model used by Mott describes the magnetic moments for ferromagnetic alloys between neighbouring elements of the iron group (Slater-Pauling curve).

These models have gradually been modified so that each contains the essential features of the other because neither is adequate in its simplest form when applied to the iron group. The direct exchange between spins in the Heisenberg model was replaced by indirect coupling via conduction electrons (Frenkel, Zener). The exchange energy favours spin alignment in ferromagnets because the Pauli exclusion principle causes the electronic charge distribution to depend on the relative orientation of spins.

Band models have been criticized (Friedel) because they could not account for effects of the local environment on an atom (and vice versa). This can be reconciled with band theory if the band structure is also allowed to depend on the local environment (Kim).

The band models mentioned so far employ the Hartree-Fock approximation. More recent refinements include attempts to incorporate

electron correlations and hybridization of overlapping bands.

2. ORDERING OF MAGNETIC MOMENTS: Paramagnetism, Antiferromagnetism and Ferromagnetism

A paramagnetic material is one which acquires a magnetization M when an external field H is applied. Magnetic moments at each atom, which are not normally aligned and do not interact with one another, are oriented by the applied field. The magnetization is described by a Brillouin function. For spin 1/2 for example the Brillouin function is given by:

$$M = N \mu \tanh(\mu H / k_B T) \tag{II-1}$$

where N is the number of moments of magnitude μ , H is the applied field, k_B is the Boltzmann constant and T is the absolute temperature. In the low field expansion, this reduces to the Curie law for the paramagnetic susceptibility χ :

$$\chi = M/H = C/T$$

where C is the Curie constant for a particular material. Because, in metals the moments do interact, this formula does not apply.

In an antiferromagnet the moments are ordered below the Néel temperature in such a way that there is no bulk moment for the material.

In a ferromagnet, the moments align in the same direction, resulting in a spontaneous magnetization below the Curie temperature T_c .

An exchange field or molecular field proportional to the magnetization was postulated by P. Weiss in 1907 to account for the

alignment of the localized spins. This model approximately describes the temperature dependence of the magnetization below the Curie temperature. Above this temperature, the material becomes paramagnetic and the susceptibility is approximately described by the Curie-Weiss law:

$$\chi = C/(T - T_c) \quad (\text{II-2})$$

The molecular field model approximates the quantum mechanical Heisenberg model wherein the spins have an interaction energy given by:

$$U = -2JS_1 \cdot S_2$$

where S_1 and S_2 are the spins on neighbouring atoms and J is called the exchange integral. It is negative for antiferromagnets and positive for ferromagnets. This model modifies the form of the susceptibility above the Curie temperature:

$$\chi = (T - T_c)^{-4/3} \quad (\text{II-3})$$

This fits experimental data close to the Curie temperature better than the Curie-Weiss law for materials that are well described by the Heisenberg model. Iron and nickel are in fairly good agreement.

3. THE STONER MODEL AND ITS APPLICATION TO FERROMAGNETIC $ZrZn_2$

Stoner's theory begins with the Hartree-Fock Hamiltonian for a single atom in a crystal:

$$H = \sum_{k\sigma} \epsilon_k n_{k\sigma} + \frac{U}{N} \sum_{k\sigma} (1 - \delta_{k,0}) \bar{n}_{k\sigma} n_{k\sigma}$$

$$= \sum_{k\sigma} \epsilon_k n_{k\sigma}$$

where k is the band index, ϵ_k is the kinetic energy term, σ is the spin, U is the average Coulomb integral and N is the number of atoms. $n_{k\sigma}$ is the number of electrons per atom in the k^{th} band with spin σ . The drastic assumption is made that the exchange integral J is the same size as the Coulomb integral U so that any electron is affected only by the average potential of electrons having the opposite spin. n_{σ} is defined by:

$$n_{\sigma} = \frac{1}{N} \sum_k n_{k\sigma}$$

so that $E_{k\sigma}$ may be written:

$$E_{k\sigma} = \epsilon_k + U n_{\bar{\sigma}}$$

The total interaction energy is then simply:

$$U n_{\uparrow} n_{\downarrow}$$

The effect of shifting the spin up and spin down halves of a single band is then considered. If a thin slice of $\rho(E_F) \cdot \delta E$ electrons were subtracted from half the band at the Fermi surface, the decrease in the band energy would be $(\rho(E_F) \cdot \delta E)(E_F - \frac{\delta E}{2})$. Adding these electrons to the other half of the band increases the energy by $(\rho(E_F) \cdot \delta E)(E_F + \frac{\delta E}{2})$ so that the total increase in band energy is $\rho(E_F) \cdot (\delta E)^2$.

The interaction energy would also change by an amount:

$$U \left[\frac{n}{2} + \rho(E_F) \cdot \delta E \right] \left[\frac{n}{2} - \rho(E_F) \cdot \delta E \right] - U \left(\frac{n}{2} \right)^2 = U \rho^2(E_F) \cdot (\delta E)^2$$

so that the total energy change is given by:

$$\Delta E = \rho(E_F) (\delta E)^2 [1 - U\rho(E_F)]$$

This results in the Stoner criterion for the formation of a stable magnetic moment:

$$U \rho(E_F) > 1$$

In this model, the presence of a narrow d band at the Fermi surface is favourable for ferromagnetism because $\rho(E_F)$ is then large.

Stoner's equations for itinerant ferromagnetism are:

$$\frac{1}{2} n(1 \pm \xi) = \int_0^{\infty} f(\epsilon, n^{\pm}) N(\epsilon) d\epsilon$$

where $f(\epsilon, n^{\pm}) = 1 / (\exp[(\epsilon - n^{\pm}) / k_B T] + 1)$

$$n^{\pm} = \mu \pm k_B \theta \xi \pm \mu_B H$$

and $\xi = M(H, T) / n \mu_B$

μ is the chemical potential, θ is a parameter relating the band splitting to the magnetization and H is the applied field.

$N(\epsilon)$ is the density of single particle states per atom per spin. The first equation indicates that as the bands shift, the number of electrons is conserved. The third equation indicates that the band splitting is proportional to the magnetization and the applied field.

A very weak itinerant ferromagnet is one for which $\xi \ll 1$, which means that the band splitting is small compared with the band width. At low temperature the equations may be expanded (Edwards and Wohlfarth) into the simple form:

$$M^2(H,T) = M^2(0,0)[1 - (T/T_c)^2 + 2\chi_0 H/M(H,T)] \quad (II-4)$$

Several properties of a very weak itinerant ferromagnet are predicted by this equation:

1) The magnetization does not saturate with field even at zero degrees. This is built into the Stoner equations because the band splitting increases with applied field.

2) M^2 plotted against H/M gives parallel straight lines for different temperatures. This has been verified experimentally by Ogawa for $ZrZn_2$. There is no $T^{3/2}$ component of the magnetization from spin wave excitation observed. The intercepts of the graph give $M^2(0,T)$.

3) $M^2(0,T)$ plotted against T^2 gives straight lines with intercepts $M^2(0,0)$ and T_c^2 . Ogawa has also verified this for $ZrZn_2$.

4) The paramagnetic susceptibility χ is predicted to have the form:

$$\chi = (T^2 - T_c^2)^{-1}$$

Experimentally, a Curie-Weiss behaviour is observed for $ZrZn_2$ at high temperature. Close to the Curie temperature the susceptibility is well fitted by $\chi = (T - T_c)^{-4/3}$. This behaviour is obtained when spin fluctuation or electron correlations are incorporated into the model (Wang et al., Moriya et al.).

4. THE SINGLE IMPURITY

The study of the problem of a single impurity atom in a ferromagnetic host was given its impetus by the Zener model in which localized d electrons interact indirectly via the s-d exchange Hamiltonian by polarizing the itinerant s electrons. At first, it looked as though the problem of how local moments form and how they behave might be simply described by a model of this type (Schwartz).

A promising experimental approach would be systematically to examine different single impurity atoms in magnetic hosts. The problem of when and how a local moment forms turns out to be much more complicated than it first appeared because it is not a property of the atomic site alone. Its formation is related to the environment, and so the formation and behaviour of a moment are not separate problems but are intimately related.

An important effect of impurities in a host was first described by Friedel: When the impurity has a different valence from the host, it provides a scattering potential for the conduction electrons. Because of the sharp cutoff in energy at the Fermi level, the surroundings of the impurity are not shielded completely from the potential and this results in charge oscillations in the host (Friedel oscillations). Essentially the same effect occurs in the spin density around an impurity as a result of the conduction electrons' coupling by the s-d interaction to the impurity local moment. These oscillations are named RKKY oscillations after Ruderman, Kittel, Kasuya and Yosida, who proposed the mechanism. The oscillations are seen experimentally

as satellite lines about the main NMR (Koi et al., Streever and Urriano, Rubinstein et al.) and Mössbauer resonances (Wertheim et al., Stearns) from near neighbours to the impurity and by broadening of the main resonances from farther neighbours. Another important means of measuring local environment effects is by diffuse neutron scattering techniques developed by Low and Collins.

Some of the impurities which form local moments in iron, cobalt and nickel hosts are: Mn, Ru, Rh, Pd, Os, Ir and Pt. None of the elements: Ti, Zr, Hf, or Zn (which are the ones pertaining to the experiments discussed in this thesis) form local moments in the same hosts. A model for the formation of a local moment has been proposed by Campbell:

5. HYPERFINE FIELDS

A hyperfine interaction is one between the electromagnetic multipoles of the nucleus and the electromagnetic fields of the atom or those of the crystal. The magnetic dipole moment interacts with magnetic fields; the electric quadrupole moment, with the electric field gradient at the nucleus. Interactions involving higher multipole moments are very small.

(a) MAGNETIC FIELDS

For a single free atom, the Dirac relativistic theory gives the interaction \mathcal{H}_D between a single electron and the nuclear magnetic dipole moment as:

$$\begin{aligned}
 \chi_D &= -g_I g_N \mu_B \mu_N \left(\frac{8\pi}{3} \vec{S} \cdot \vec{I} \delta(\vec{r}) + \frac{(\vec{L} - \vec{S}) \cdot \vec{I}}{|\vec{r}|^3} + \frac{3(\vec{S} \cdot \vec{r})(\vec{I} \cdot \vec{r})}{|\vec{r}|^5} \right) \\
 &= g_I \mu_N \vec{I} \cdot \vec{H}_{hf} \\
 &= g_I \mu_N I |\vec{H}_{hf}| \cos \theta
 \end{aligned}
 \tag{II-5}$$

where \vec{H}_{hf} is the hyperfine magnetic field,

\vec{L} is the electron orbital angular momentum,

\vec{S} is the electron spin angular momentum,

\vec{I} is the nuclear total angular momentum,

μ_B is the Bohr magneton,

μ_N is the nuclear magneton,

g, g_I are the electronic and nuclear g factors respectively

and $\cos \theta$ is the projection of \vec{I} on the Z axis, taken to be parallel to \vec{H}_{hf} .

The last two terms are dipolar interactions which are zero for s electrons. The first term is non-zero only for s electrons and is called the Fermi contact term. In transition metals, where the orbital angular momentum is largely quenched, this term accounts for most of the hyperfine magnetic field.

Additional contributions to the magnetic field at the nucleus are the external field H_{ext} , the Lorentz field H_L arising from all the magnetic moments induced in the sample, and the demagnetizing field $-4\pi DM$ from polarization at the surface of the sample. D is the demagnetizing factor which depends on the shape of the sample. The total magnetic field at the nucleus is called

the effective field and is given by:

$$H_{\text{eff}} = H_{\text{hf}} + H_{\text{ext}} + H_L - 4\pi DM \quad (\text{II-6})$$

For the transition metals, the origin of the hyperfine field is mostly the Fermi contact term. This is proportional to the net unpaired spin density of s electrons at the nucleus. There are two components: core polarization (CP) and conduction electron polarization (CEP). The interaction of the d electrons with the inner core s electrons changes the spatial distribution of their spin in such a way that the polarization at the nucleus is negative (anti-parallel to the d electrons). The conduction electrons, which have most of their wavefunctions outside the d shell, have positive spin polarization at the nucleus but negative polarization outside the d shell. The CP term dominates so that in pure iron, cobalt and nickel the hyperfine fields are negative (relative to the applied field).

(b) ELECTRIC FIELD GRADIENTS

A field gradient will exist at the nucleus of an atom in a crystal lattice if the neighbouring atoms are not distributed about it with cubic symmetry. For an axially symmetric field gradient $\frac{\partial E_z}{\partial z}$, the electric quadrupole interaction energy is given by:

$$E_Q = \frac{3m^2 - I(I+1)}{4I(I+1)} eQ \frac{\partial E_z}{\partial z}$$

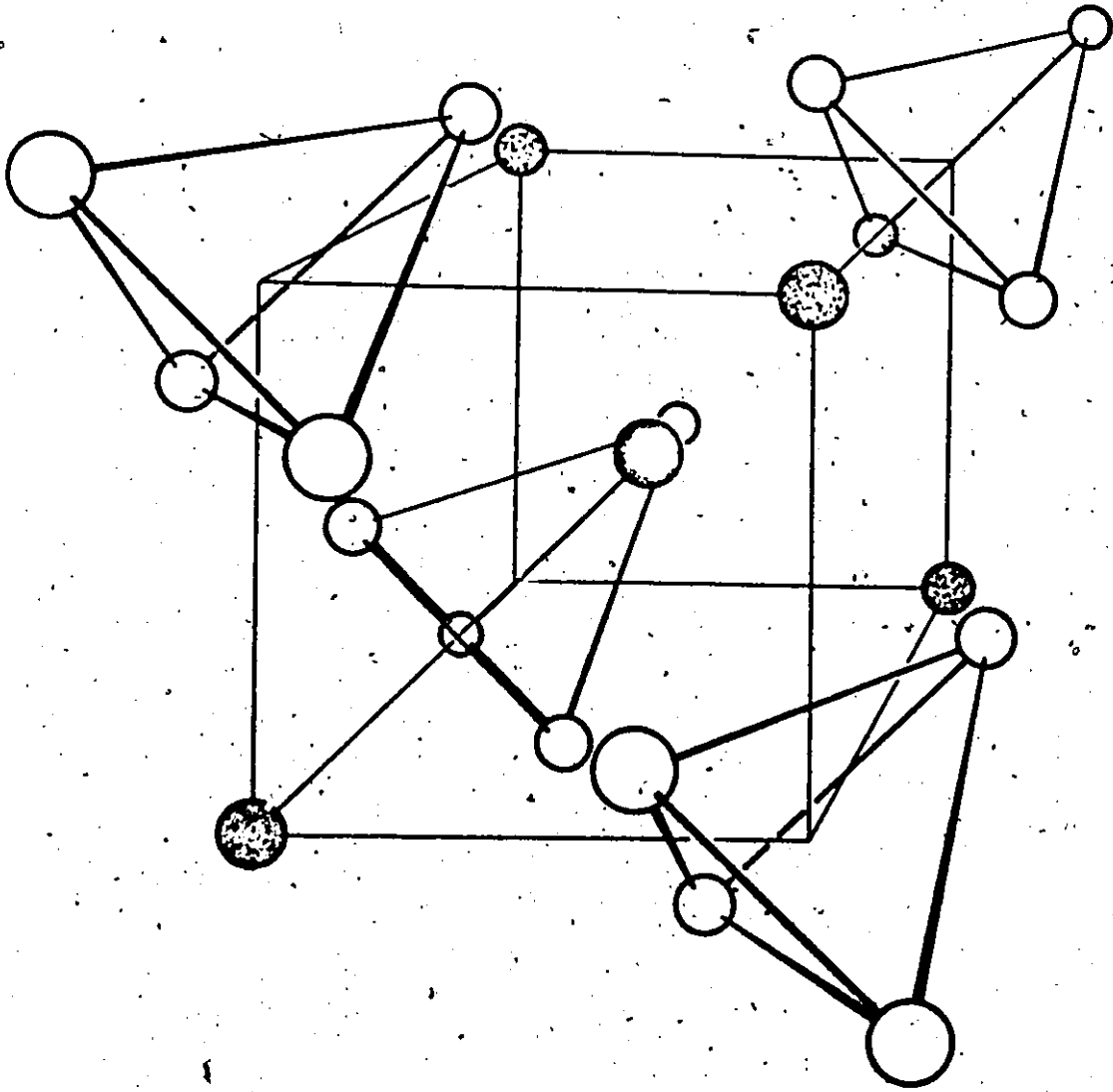
where m is the magnetic substate of the state I and Q is the spectroscopic quadrupole moment for the nucleus in the state I . (For the $I = 5/2^+$ state of ^{181}Ta , $Q = 2.51 \pm 0.15$ barns, Metz and Bodenstedt).

In the presence of a field gradient, the charge distribution of an atom becomes polarized. For large atoms this produces a field gradient at the nucleus which is much greater than the original one causing the polarization. The amplification $1-\gamma_{\infty}$ is called the Sternheimer anti-shielding factor. For Tm^{5+} , $\gamma_{\infty} = -61$ (Feilock and Johnson). Because of the cubic symmetry about the impurity site (Fig. II-1), no field gradient is expected except for those caused by lattice defects.

Figure II-1

Point Symmetry About Ta Impurity Atom

The dark circle in the centre represents the tantalum impurity atom, the grey circles - the zirconium, and the open circles arranged in tetrahedra - the zinc atoms.



CHAPTER III

γ - γ ANGULAR CORRELATIONS

This thesis is concerned with the measurement of hyperfine magnetic fields at ^{181}Ta nuclei located at zirconium sites in ferromagnetic ZrZn_2 . The method which was used to measure these fields is called time-differential perturbed angular correlations. The angular correlation of the gamma rays emitted by the nucleus is perturbed by the influence of both magnetic fields and electric field gradients at the nucleus. This chapter describes the form of the perturbed angular correlation for different experimental situations. Derivations of the formulas quoted may be found in the review article by Frauenfelder and Steffen. Only directional correlations will be considered, which means that the detectors are insensitive to the circular polarization of the gamma rays.

1. UNPERTURBED ANGULAR CORRELATION

When a nucleus undergoes transitions from initial to intermediate to final states having spins I_1 , I and I_2 , two cascade gamma rays γ_1 and γ_2 are emitted having multipolarities L_1 and L_2 . The directional correlation between the gamma rays is given by:

$$W(\theta, t) = \left[1 + \sum_{\substack{k=2 \\ k \text{ even}}}^{k_{\text{max}}} a_{k k k} Q_k P_k(\cos \theta) \right] \exp(-t/\tau)$$

where θ is the angle between the detectors and t is the time between the emissions of the gamma rays. The Q_k 's are the solid angle attenuation factors and the P_k 's are the Legendre polynomials. τ is the mean life of the intermediate state and $k_{\max} = \min(2I_1, 2I_2, 2L_2)$. For the 182 keV state of ^{181}Tm , L_2 is 2 so that the maximum value of k is 4. For practical purposes this is always the maximum value of k because transition probabilities for higher multipolarities than $L=2$ are very small.

2. PERTURBED ANGULAR CORRELATIONS

Extranuclear perturbations may result in a time dependence of the correlation function other than the exponential one. The perturbation may be described by the interaction of the electromagnetic multipole moments of the nucleus and the hyperfine fields at the nucleus which are caused by its environment. Only two types of interactions are significantly strong to have been detected by angular correlation experiments: the interaction of a magnetic field \vec{H} with the nuclear magnetic dipole moment $\vec{\mu}$, and the interaction of the electric field gradient $\partial^2 E / \partial r^2$ (a tensor) with the electric quadrupole moment Q of the nucleus.

(a) MAGNETIC FIELDS

For a magnetic field oriented perpendicular to the counter plane, the perturbed angular correlation is given by:

$$W_2(\theta, H, t) = \left[1 + \sum_{k=2,4} a_k Q_k P_k(\cos(\theta - \omega_L t)) \right] \exp(-t/\tau)$$

or equivalently

$$W_{\perp}(\theta, H, t) = [1 + \sum_{k=2,4} b_k \cos k(\theta - \omega_L t)] \exp(-t/\tau) \quad (\text{III-1})$$

$$\text{where } b_2 = \frac{\frac{3}{4} a_2 Q_2 + \frac{5}{16} a_4 Q_4}{1 + \frac{1}{4} a_2 Q_2 + \frac{9}{64} a_4 Q_4} \quad \text{and } b_4 = \frac{\frac{35}{64} a_4 Q_4}{1 + \frac{1}{4} a_2 Q_2 + \frac{9}{64} a_4 Q_4}$$

For the 452 keV state of ^{181}Ta , $a_2 = -0.29$ and $a_4 = -0.07$. For the experiments in this thesis $Q_2 = 0.84$ and $Q_4 = 0.4$ so that $b_2 = -0.21$ and $b_4 = -0.02$.

The Larmor precession frequency is given by:

$$\omega_L = -g \mu_N H / \hbar \quad (\text{III-2})$$

where g is the g factor for the intermediate nuclear state ($g = 1.32 \pm 0.03$ for the 452 keV state of ^{181}Ta), μ_N is the nuclear magneton and \hbar is Planck's constant $/2\pi$. Figure III-1 shows the decay scheme for ^{181}Ta .

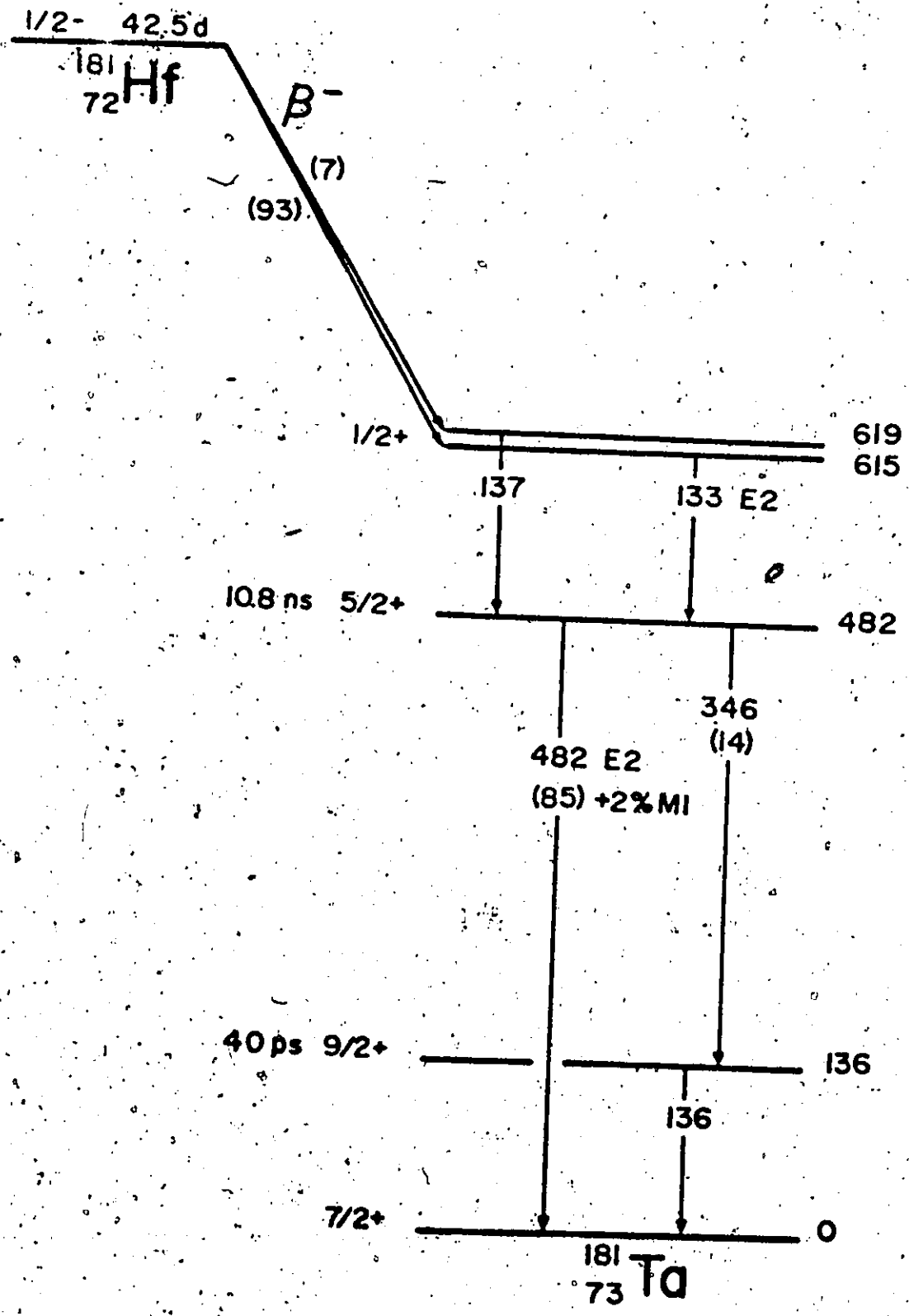
The largest time dependent term is the b_2 term so that the dominant frequency observed in $W_{\perp}(\theta, H, t)$ is $2\omega_L$ or twice the precession frequency. This is because there are two maxima and minima in the correlation pattern (Fig. VI-1) which pass a detector for a single precession of the nucleus.

For detectors at 180° or 90° and the magnetic field in the counter plane at 45° or 135° , the single Larmor frequency is observed. If the source is an unmagnetized ferromagnet (in which the field throughout has random directions), then a component of both the single and double frequencies is observed.

Figure III-1

Level Scheme of ^{181}Ta

The state which is of interest in this thesis is the one with the half-life of 10.8 ns. The coincidences looked for are those between the 133 keV and 482 keV gamma rays.



(b) ELECTRIC FIELD GRADIENTS

For the electric quadrupole interaction the rate of precession of the nucleus depends on its orientation. Because of this, the angular correlation pattern does not simply rotate as it does for magnetic interactions. In the case of an axially symmetric electric field gradient, the quadrupole frequency is defined by:

$$\omega_Q = - \frac{eQ(\partial E_z / \partial Z)}{4I(2I-1)\hbar} \quad (\text{III-3})$$

where Q for the $5/2^+$ state of ^{181}Ta is 2.51 ± 0.15 barns (Netz and Bodenstedt). The angular frequency is given by:

$$\omega_0 = \begin{cases} 3\omega_Q & \text{for integer } I \\ 6\omega_Q & \text{for half-integer } I \end{cases} \quad (\text{III-4})$$

The angular correlation is given by:

$$W(\theta, \frac{\partial E_z}{\partial Z}, t) = [1 + \sum_{k=2,4} I_k \frac{a_k Q G_k(t) P_k(\cos \theta)}{\gamma_k}] \exp(t/\tau)$$

where $G_k(t)$ is the perturbation factor which contains all the available information about the perturbation.

In a polycrystalline source, $G_k(t)$ is given by:

$$G_k(t) = \sum_n S_{kn} \cos(n\omega_0 t)$$

where the coefficients S_{kn} depend on the value of I . For ^{181}Ta

($I = 5/2$ for the 482 keV state) for example:

$$G_2(t) = \frac{1}{5} + \frac{13}{35} \cos(\omega_0 t) + \frac{2}{7} \cos(2\omega_0 t) + \frac{1}{7} \cos(3\omega_0 t)$$

The first term, $1/(2k + 1)$ is called the "hard core" value. For static perturbations $G_k(t)$ has a lower limit which is never less than the hard core value. (The lower limit occurs gradually because the nuclei are not all in exactly identical field gradients so that their precessions get out of phase).

Experimentally the two types of interactions are easily distinguishable even when the differences in the shape of the correlation pattern are not clear. This is because, in the case of electric quadrupole interactions, the pattern is symmetric about 180° while for magnetic interactions perpendicular to the counter plane it is not.

More complicated patterns develop when the electric field gradient is not axially symmetric or when there are mixed magnetic and electric interactions.

(c) TIME DEPENDENT PERTURBATIONS

When the extranuclear perturbations are time dependent, $G_k(t)$ may relax to zero. There are several models for randomly fluctuating interactions (Abragam and Pound, Dillenburg and Maris, Gabriel, Blum). According to the Abragam-Pound model, random quadrupole interactions in liquids give rise to a perturbation factor:

$$G_k(t) = \exp(-\lambda_k t)$$

where λ_k is proportional to the correlation time τ_c which is approximately 10^{-11} sec in liquids. As long as $\tau_c \ll \tau_H$ (the nuclear mean life) then $G_k(t) \approx 1$ so that the unperturbed correlation is observed. (It is also necessary that $\omega\tau_c \ll 1$).

3. TIME RESOLUTION

If the time dependence of the coincidence count rate is given by:

$$W(t) = (1 + b \sin \omega t) \exp(-\lambda t) \quad \text{for } t > 0$$

and the time resolution of the apparatus by:

$$\rho(t'-t) = \frac{1}{2\pi\sigma} \exp[-(t'-t)^2/2\sigma^2]$$

then the convolution of the two expressions gives the measured correlation:

$$\begin{aligned} C(t') &= \int_{-\infty}^{\infty} W(t) \rho(t'-t) dt \\ &= [1 + b \exp(-\omega^2 \sigma^2 / 2) \sin \omega(t' - \sigma^2 \lambda)] \exp(\sigma^2 \lambda^2 / 2) \exp(-\lambda t') \end{aligned}$$

This is correct only for $t' > 0$ because $W(t)$ should actually be zero for $t < 0$. If σ is small, the main effect is that the amplitude of the oscillations is attenuated. The new amplitude is given by: Δ

$b' = b \exp(-3.5(2\tau/T)^2)$ where $\tau = 1.18 \sigma$, T is the period and 2τ is the resolution full width half maximum (FWHM).

For the experiments in this thesis $2\tau = 1.6$ ns and $T > 20$ ns so that the effect can be neglected (3%).

CHAPTER IV
EXPERIMENTAL ARRANGEMENT

1. THE APPARATUS

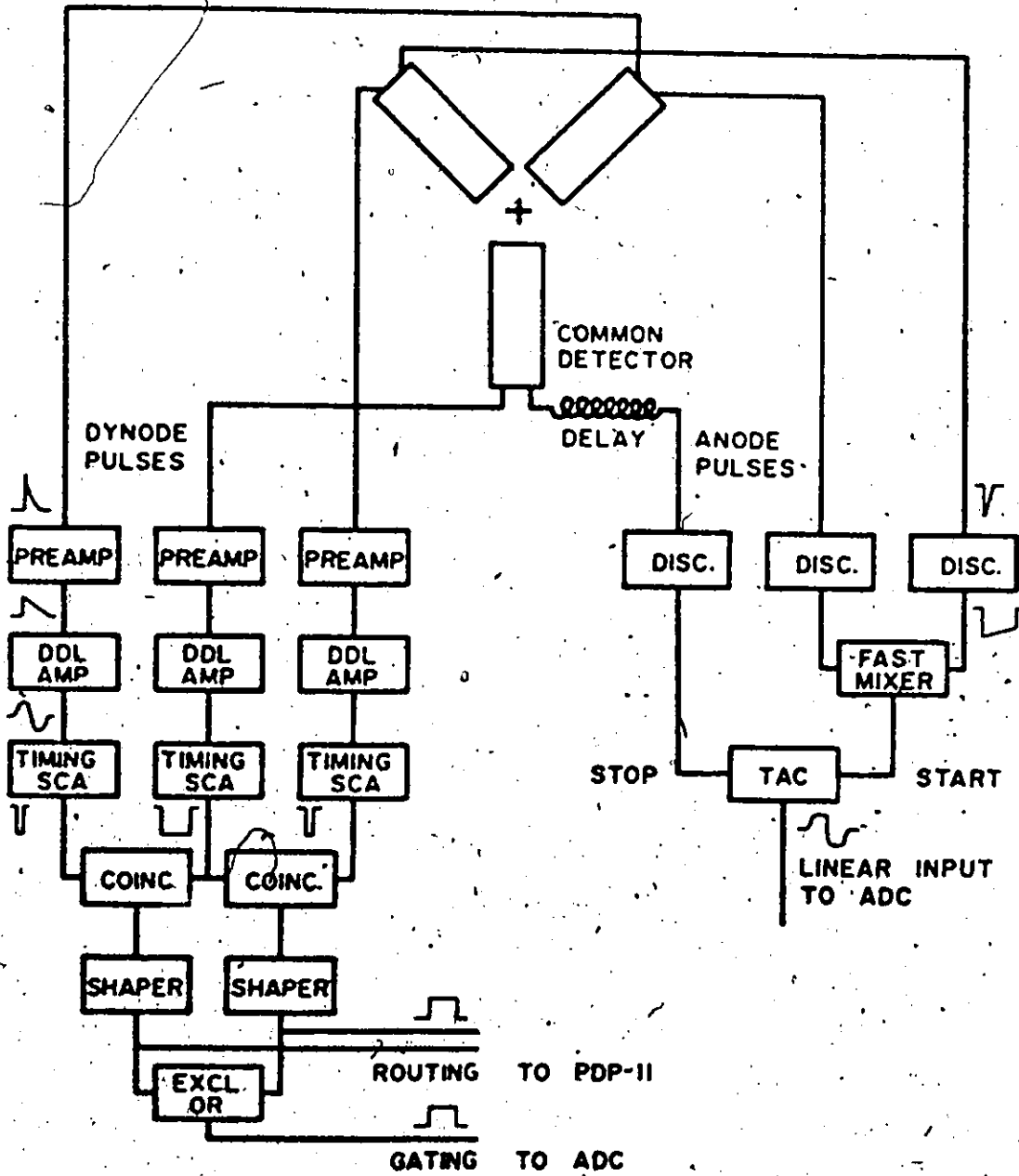
Figure IV-1 shows schematically how time spectra were generated and collected. A single time-to-amplitude converter (TAC) was started by pulses from the anodes of two RCA 8575 photomultiplier tubes using 1" x 1/2" sodium iodide scintillators to detect the 482 keV gamma ray in the 133-482 keV cascade in ^{181}Tm . The stop came from an RCA 8850 tube with a 1" x 1/4" sodium iodide crystal detecting the 133 keV gamma ray (artificially delayed pulse). Single channel analyzer (SCA) pulses from the energy peaks were exclusively OR'ed and used to route the two TAC spectra. These were collected by a PDP 11/05 computer, programmed for on-line data analysis. The program is listed in the appendix to the thesis.

(a) SCINTILLATORS, PHOTOMULTIPLIER TUBES AND TUBE BASES

With the electronics used, the time resolution with plastic scintillators (Naton 136) for 511 keV gamma rays from ^{22}Na was better than 0.5 ns (FWHM). For sodium iodide NaI(Tl) the resolution was about 1 ns. For the experiments in this thesis, good time resolution was not crucial and NaI(Tl) was chosen. The photoelectric cross-section is much higher than for plastic so that the energy resolution is much better. This is necessary for resolving the 482 keV gamma ray

Figure IV-1

Schematic Diagram of The Apparatus



(85%) of ^{181}Ta from the 346 keV (14%) which would give a large prompt peak in the time spectrum.

The RCA 8850 photomultiplier was used for the 133 keV gamma ray because it has a higher gain than the RCA 8575. Both of these tubes are especially good for experiments that require good time resolution.

The tube base is essentially a voltage divider used to provide the voltages for the dynodes of the photomultiplier tube. Pains were taken to minimize the capacitance of the base so that the anode pulse would have the fastest possible rise time. In the first stage and the last three stages of the dynode chain, Zener diodes were used to maintain constant voltages as the count rate changed. The cathode was run at -2600V with respect to the anode and the tube was surrounded by a shield at -1300V. The slow pulses used for energy selection and coincidences of the appropriate gamma rays were taken from the ninth dynode. The fast timing pulses were taken from the anode. A constant room temperature is desirable over the duration of an experiment (Wagner and Forker). Zero shifts in the time spectrum of up to 0.2 ns accompany changes in the room temperature of about 10 degrees C.

(b) DISCRIMINATORS

The electrons arriving at the anode are Poisson distributed in time so that the resolution varies as the square root of the number of electrons. For this reason it is desirable to detect the part of the pulse from the first photoelectron. The purpose of the discriminator is to do this and produce a pulse with a fast rise

time to drive the time-to-amplitude converter (TAC).

The discriminators were constructed using a uA710 high speed differential comparator (Fairchild). The output pulse (about 10 ns/V) is triggered by the leading edge of the anode pulse close to the noise level which was less than 10 mV. The time resolution obtained for 133 keV and 482 keV gamma ray windows on the energy spectrum of ^{22}Na was 1.6 ns FWHM.

2. TIME CALIBRATION

The time calibration of the system was accomplished by a circuit developed by Boulter et al. It employs crystal oscillators to produce a start pulse for the TAC and stop pulses at preset intervals. The spectrum collected consists of time spikes which are equally spaced if the system is linear. The calibrator has been checked using a frequency counter several times over a period of years and is constant within 14 parts per million.

3. NON-LINEARITY

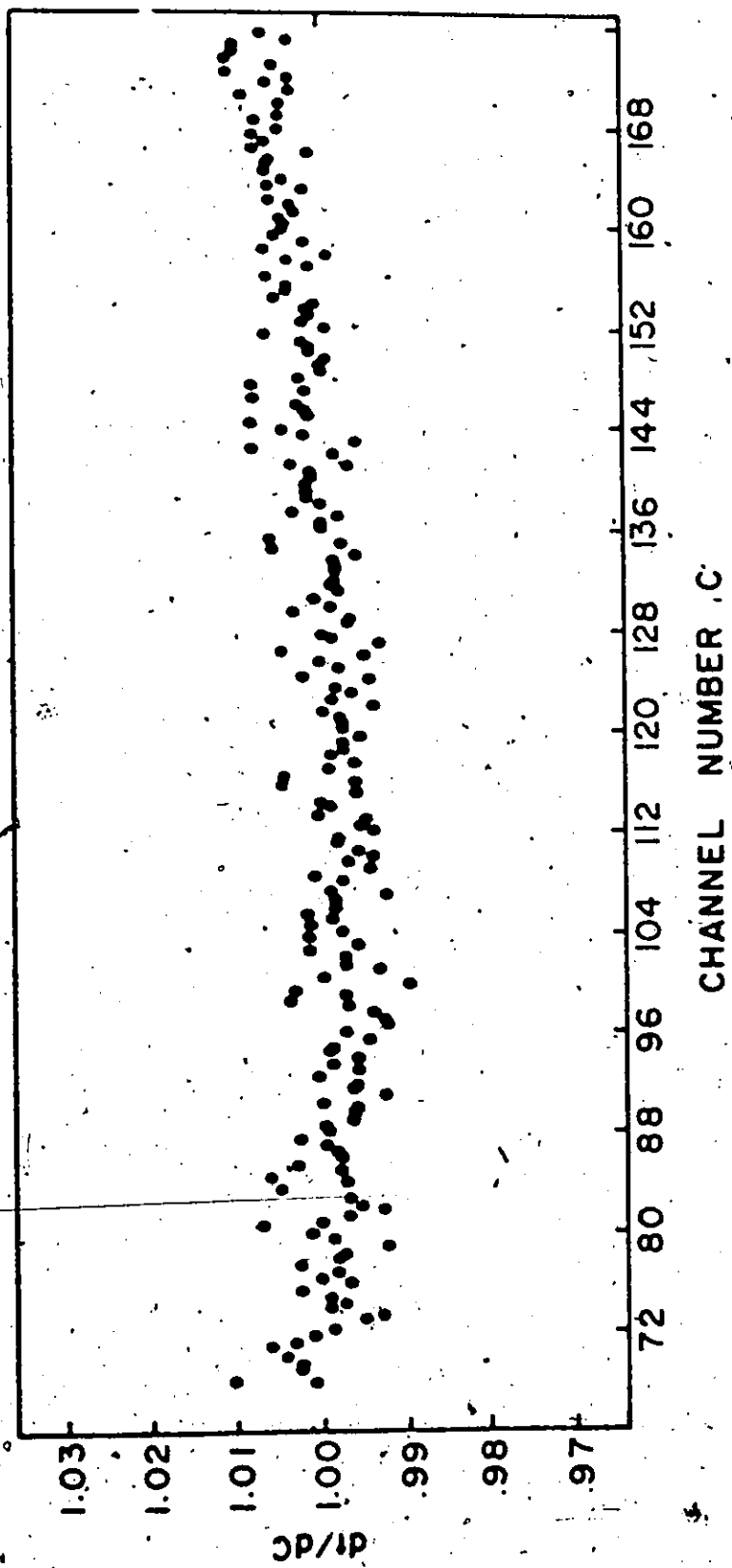
To measure the non-linearity of the system (including both the TAC and the analogue-to-digital converter (ADC)), a spectrum is generated which is flat for a linear system. The spectrum actually acquired is called the differential non-linearity (DNL) curve dt/dc . Each point shows relatively how much time t corresponds to its particular channel C . The DNL curve is generated by starting the TAC with random pulses (using a radioactive source and photomultiplier tube). A pulser is used to stop the TAC and the interval between

Figure IV -2

Differential Non-Linearity Curve

The time spectra from actual experiments were acquired in the region of the DNL curve from 99.7% to 100.3%, which was approximated by a straight line.

2



pulses must be longer than the time scale of the TAC. (Using a source to stop the TAC gives an exponentially decreasing curve). Spectra from experiments are corrected by dividing by the DNL curve (or fit to it) channel by channel:

$$N(t) = N(C) / (dt/dc)$$

$$\text{where } t = \int (dt/dc) dc$$

$N(C)$ is the number of counts in channel C , $N(t)$ is the corrected number of counts at time t . Figure IV-2 is a DNL curve generated for the apparatus used for the experiments in this thesis. Spectra were acquired in the region of the DNL curve from about 99.7% to 100.3%, which was approximated by a straight line.

The lifetime of the 482 keV state of ^{181}Ta was measured, using a liquid source made by dissolving neutron activated hafnium metal in a concentrated HF solution, so that the correlation would be unperturbed. The time calibration was done three times over the duration of the experiment and was determined within 0.2%. Figure IV-3 shows the time spectrum from the decay of the 482 keV state. The DNL correction changed the lifetime by 0.3%. The measured half-life was 10.76 ± 0.05 ns which agrees well with that of Love et al. who used the same calibrator but otherwise different apparatus and obtained a value of: $T_{1/2} = 10.81 \pm 0.05$ ns.

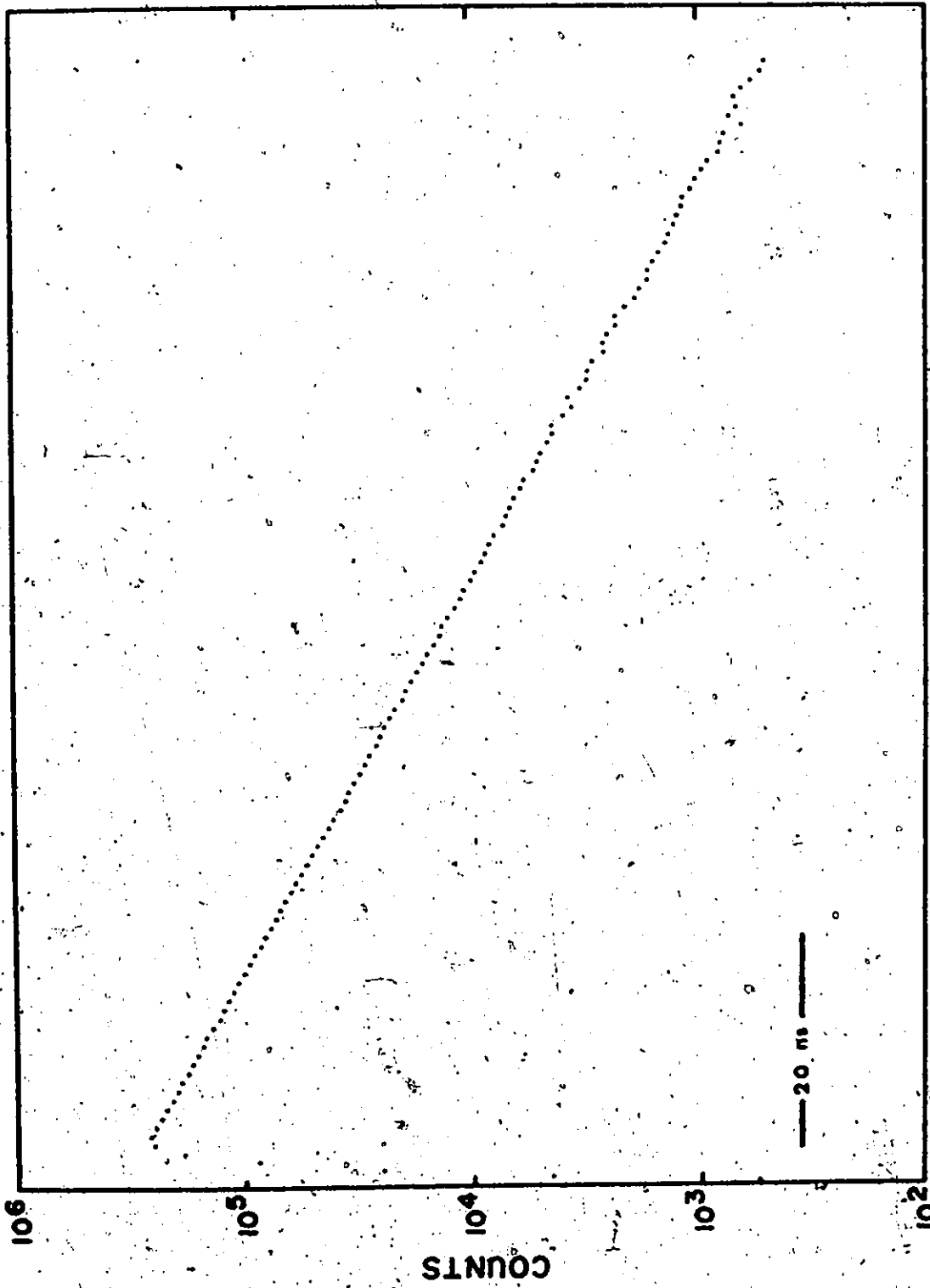
4. THE MAGNET

To provide the external polarizing field on the ZrZn_2 sample, a small permanent magnet was constructed. It consisted of

Figure IV-3

Time Spectrum for the Decay of the 482 keV State
in ^{181}Ta

5



TIME

20 ns

two rods of an alnico alloy one quarter inch in diameter and about an inch long each. These were separated by an aluminum washer 0.0020 ± 0.0005" thick with a 1/8" diameter hole for the samples.

The narrowness of the tail of the liquid helium cryostat, into which the magnet had to fit, did not permit construction of a return path for the field of the magnet.

The field inhomogeneity (Zijlstra) was calculated for the volume of the magnet cavity. The normalized axial component of the field, H_z , is given by:

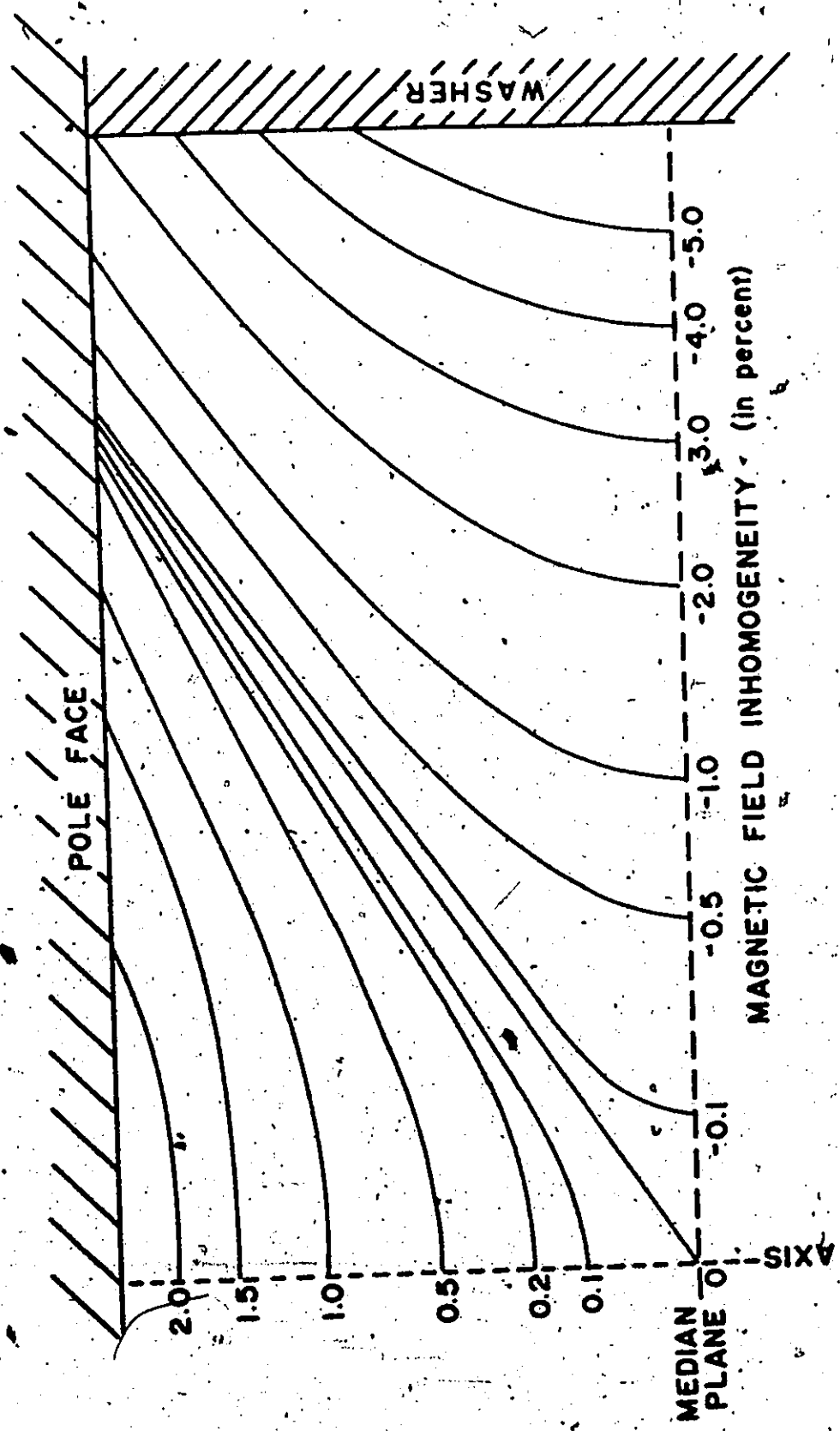
$$H_z = 1 + \left[1 - \frac{\alpha}{(\alpha^2 + 1)^{1/2}} \right]^{-1} \left[\frac{3\alpha}{2(\alpha^2 + 1)^{5/2}} \left(\frac{r}{r_0} \right)^2 P_2(\cos \theta) + \frac{6\alpha^3 - 4.5\alpha}{24(\alpha^2 + 1)^{9/2}} \left(\frac{r}{r_0} \right)^4 P_4(\cos \theta) + \dots \right]$$

where r_0 is the radius of the magnet, Z is the distance from the centre point to a pole face, $q = Z/r_0$, r is the radial distance from the axis to any point in the cavity, θ is the angle between a line joining this same point to the centre point and the magnet axis, and P_2 and P_4 are the Legendre polynomials. Figure IV-4 shows the calculated lines of equal H_z . The largest deviation from the central value is about -6% near the edge of the cavity and the volume weighted mean field is 1.8% lower than the central value. The average absolute value of the deviation (volume weighted) from the mean field is 1%.

The field was measured over the median plane of the cavity using a Hall probe gaussmeter. The magnet was taken apart, reassembled,

Figure IV-4

Calculated Magnetic Field Inhomogeneity For the Magnet
Used in the Hyperfine Field Measurements



remagnetized, and the field remeasured several times. The central value obtained for the field was 3.02 ± 0.05 kG. Where the edge of the cavity would be, the field dropped to 2.94 kG which is less than the calculated decrease (to about 2.85 kG). The Hall probe was checked by measuring a 3.00 kG field in a large accurately calibrated electromagnet. The probe was found to be accurate to better than 0.05 kG. The value of the mean field used was 3.0 ± 0.1 kG. The effect of the spread in field (-1% to $+1\%$) is too small to be noticed in the angular correlation measurements in this thesis where only a few oscillations are detected.

5. THE DEMAGNETIZING FACTOR

The demagnetizing factor L (refer to Section II-5a) for a sample filling the magnet cavity is 0.46, giving a demagnetizing field of $-0.46H$ where H is the magnetization of the sample at 3 kG applied field.

CHAPTER V

SAMPLE PREPARATION AND ANALYSIS

1. SAMPLE REPRODUCIBILITY

The method of preparing $ZrZn_2$ has been to press the metal powders into a pellet and to sinter it at about $915^\circ C$ for several days. Many researchers have found that the magnetization and Curie temperature are not reproducible from sample to sample. Knapp et al. have found that the cubic Laves phase (Fig. I-1) forms over a range from $ZrZn_{1.8}$ to $ZrZn_{2.0}$. The maximum Curie temperature of $26^\circ K$ occurs at $ZrZn_{1.9}$ for samples made at $965^\circ C$. If the samples are made at $965^\circ C$, the Curie temperature is only about $16^\circ K$ for $ZrZn_{2.0}$ whereas if they are made at $700^\circ C$, the Curie temperature is again about $26^\circ K$ and varies only by about two degrees over the range of stoichiometry from $ZrZn_{1.8}$ to $ZrZn_{2.0}$. They conclude that the cubic Laves phase contains only $ZrZn_{1.9}$ when made at $700^\circ C$. Other reasons for the lack of reproducibility are the presence of impurities and strains. There are usually traces of other phases, particularly $ZrZn_3$ in all samples. (phase diagram, Fig. V-1).

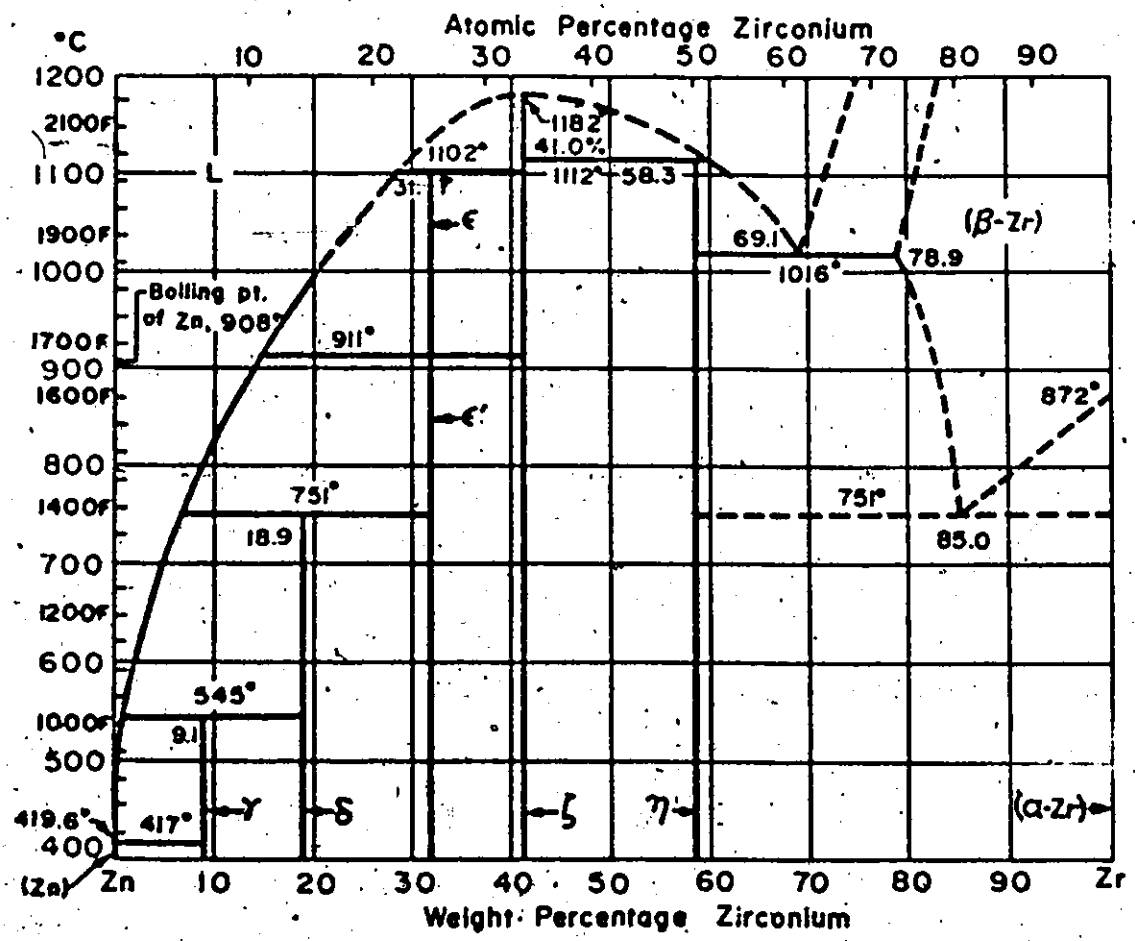
In view of the reproducibility problem then, it is evident that hyperfine field measurements in $ZrZn_2$ should not stand alone but that as much information as possible ought to be obtained about the condition of each sample. Three types of experiment were carried out: powder X-ray analysis to determine the phases present in the



Figure V-1

Phase Diagram for Zirconium - Zinc

Zn-Zr Zinc-Zirconium



samples, neutron activation analysis to ascertain the actual zinc concentrations, and Mill magnetization measurements. The magnetizations were corrected because the measured value averages over the whole sample, including non-magnetic portions.

2. SAMPLE PREPARATION

The metal powders used in the preparation of the $ZrZn_2$ samples were obtained from Alfa Inorganics Ltd. The purities were:

Hf	99.8%	(Fe 1800 ppm, Ti 300 ppm, Zr 4.5%)
Zr	99.9%	(Fe 450, Ta 150, Ni 50, Hf 60, O 900)
Ti	99.95%	(Fe 40 ppm, O 300 ppm)
Zn	99.999%	(Fe 1 ppm)

In order to measure the hyperfine field at ^{181}Ta nuclei in $ZrZn_2$ at least 2% of the zirconium was replaced with hafnium powder which had been neutron activated to produce the radioisotope ^{181}Hf .

It was hoped that the hafnium atoms would diffuse throughout the $ZrZn_2$ lattice to the zirconium sites.

Pellets 3.8 mm in diameter and about 5 mm long were made by pressing the metal powders together under a weight of 700 lbs. The pellets weighed about 150 mg. They were then sealed in evacuated quartz and sintered at different temperatures for various lengths of time. The furnace, which maintained its temperature within 3 degrees C, was constructed from a diffusion pump heater.

In all, 14 samples were prepared and numbered 1 to 14. 9 samples discussed in this thesis are designated by either their numbers or nominal compositions. Some of the samples were made at

916°C and others at 730°C. Besides this, two different mixing procedures were followed. The first samples were made by simply pressing the constituent powders together and relying on diffusion to distribute the hafnium in the lattice. No measurable hyperfine field (45kOe) was observed for samples made in this way at 730°C for sintering times less than a month, and none were observed for samples made at 916°C if the sintering time was less than a week. It was felt that the diffusion rate of the hafnium might be the reason. The finished samples retained their cylindrical shape, suggesting that only the zinc atoms are very mobile. In the sealed quartz UO_2 does not melt until 1180°C.

The second procedure was to melt the hafnium and zirconium (and titanium for some samples) together at the beginning under vacuum with an electron beam. The ingots were filed lightly and the iron from the file was removed from the powder, first with a magnet, then by etching with a 50-50 mixture of formic acid and superoxal (30% hydrogen peroxide). (Knapp et al.). The dried powder was then irradiated in the reactor before the zinc was added to make the pellet. The samples were sintered at 730°C for one week. The outer surface of every pellet was filed and only the inner portion was used. They were a uniform dull grey colour inside, had a grainy texture and crumbled easily. A cylindrical sample was cut to fit the cavity of the magnet used in the TDPAC experiments. The sample numbers, nominal compositions, method of preparation and actual zinc concentration are summarized in Table V-1.

NEUTRON ACTIVATION ANALYSIS

The neutron activation analyses were the last experiments carried out but will be discussed now for continuity.

About 30 mg of the centre portion of each sample was sealed in fine quartz tubes and neutron activated (for 20 hours at 3×10^{13} neutrons/cm²/sec) all together with a dummy sample containing accurately weighed (± 0.05 mg) amounts of zirconium, hafnium and zinc.

The intensity of the 1.115 MeV gamma ray from ⁶⁵Cu after the β^+ decay of ⁶⁵Zn ($t_{1/2} = 245$ days) and the intensity of the 0.724 MeV gamma ray from ⁹⁵Zb after the β^- decay of ⁹⁵Zr ($t_{1/2} = 5.5$ days) were measured. This was done for each sample before and after the neutron activation (since the zirconium had previously been activated in most of the samples so that the result of this must be subtracted from the final activity). The relative intensity of each gamma ray to that of the dummy sample was measured using two GeLi detectors 1 metre apart, counting each sample for an hour. The two detectors independently gave consistent zinc concentrations, which are listed in Table V-1. (The fact that some zirconium has been replaced with hafnium or titanium has been taken into account). All the samples appear to have excess zinc. Even the ones made at 916°C could not have as much zinc as was measured all in the ZrZn₂ phase. If the assumptions are made that the samples made at 700°C have 1.9 zinc atoms per zirconium site; those made at 916°C have 2.0 Zn atoms per zirconium site, and that the zinc left over is taken up by the

TABLE V-1 SUMMARY OF SAMPLE PREPARATIONS AND ZINC CONCENTRATIONS

SAMPLE NO.	NOMINAL COMPOSITION	SAMPLE PREPARATION	ACTUAL ZINC CONCENTRATION (AS MEASURED)
1	Zr .98 Hf .02 Zn 2.0	910°C 1 week) Hf diffused in	2.14 ± 0.06
4	Zr .90 Hf .10 Zn 1.9	730°C 1 month) Hf diffused in	2.04
5	Zr .85 Hf .15 Zn 1.9	910°C 1 month)	2.13
7	Zr .85 Hf .15 Zn 1.9		2.05
8	Zr .98 Hf .02 Zn 1.9		1.91
10	Zr .98 Hf .02 Zn 1.8		2.15
11	Zr .88 Ti .10 Hf .02 Zn 1.9	730°C 1 week Hf melted in	2.15
12	Zr .80 Hf .20 Zn 1.9		2.02
14	Zr .80 Ti .18 Hf .02 Zn 1.9		2.15

NOTE: There is a systematic error of another ±0.06 in the zinc concentration as a result of the weighing uncertainty and statistical uncertainty for the durry sample.

ZrZn₃ phase (the main impurity as demonstrated by the X-ray analysis), then the proportion of the sample which is magnetic can be estimated.

In sample #1, for instance:

$$\text{ZrZn}_{2.24} = x(\text{ZrZn}_{2.0}) + y(\text{ZrZn}_3)$$

$$x + y = 1$$

so that $x = .76$

The result for each sample is recorded in Table V-2.

4. X-RAY ANALYSIS

ZrZn₂ was determined by Pietrokovsky in 1954 as having the cubic Laves structure (Fig. I-1.) TiZn₂ does not have the same structure because the Ti atoms are too small. This is presumably why the magnetization of Zr_{1-x}Ti_xZn₂ begins to drop off at X = .2 after initially increasing.

Powder X-ray photographs were made and a portion of the spectrum is shown for each sample in Fig. V-2. The lines at 2.63 Å, 2.23 Å and 2.13 Å indicate the d-spacings for the [2,2,0], [3,1,1] and [2,2,2] planes respectively in ZrZn₂. Lines at 2.34 Å and 2.03 Å belong to the [2,2,2] and [4,0,0] planes of the cubic ZrZn₃ phase. The two impurity lines in sample #8 have not been identified. Although the central portion of the pellets visually appeared to be uniform, the tiny part of each sample that was X-rayed might not be entirely representative of the condition of the whole sample. The proportion of each sample that is in the ZrZn₂ phase has been estimated by the ratios of peak areas in the spectra. The numbers were normalized to

Figure V-2

A Portion of the Powder X-Ray Spectra

for the $ZrZn_2$ samples described in this thesis. The lines with lattice spacings corresponding to prominent lines of $ZrZn_2$ (solid lines) and $ZrZn_3$ (broken lines) are labelled.



the proportion obtained for sample #10 using neutron activation and are listed in Table V-2.

5. BULK MAGNETIZATION MEASUREMENTS

Before the X-ray or neutron activation analyses were undertaken, bulk magnetization measurements were made with a vibrating sample magnetometer on the whole samples which had been used to determine the hyperfine fields. Figs. V-3 and V-4 show the magnetization plotted against field. The magnetization was also measured as a function of temperature at 750 G and at 2000 G. Figs. V-5 and V-6 are plots of $M^2(0,T)$ vs. T for the samples which had a measurable Curie temperature. The data were analyzed along the lines suggested by the Stoner theory (Chapter II, Section 3). The values of $M^2(0,T)$ were obtained by extrapolating $M^2(H,T)$ vs. H/M to zero field. The plots shown deviate from a straight line at high temperatures, probably because of this extrapolation. At high temperatures, M is low so that any systematic errors become more pronounced in H/M . Better results would probably have been obtained if the temperature dependence of M had been measured at some more fields higher than 2000 G. The values obtained for $M^2(0,0)$ are quite consistent with the values of $M^2(0,H)$ found by extrapolating the graphs of M vs. H . The Curie temperatures and uncorrected values of $M^2(0,0)$ are recorded in Table V-2.


6. CORRECTION TO THE MAGNETIZATION

Because not all the sample consisted of the magnetic $ZrZn_2$ phase, the measured magnetization (in Bohr magnetons per zirconium

Figure V-3

The Measured Bulk Magnetization

as a function of field for samples 8, 1 and 10 (from
the top down).



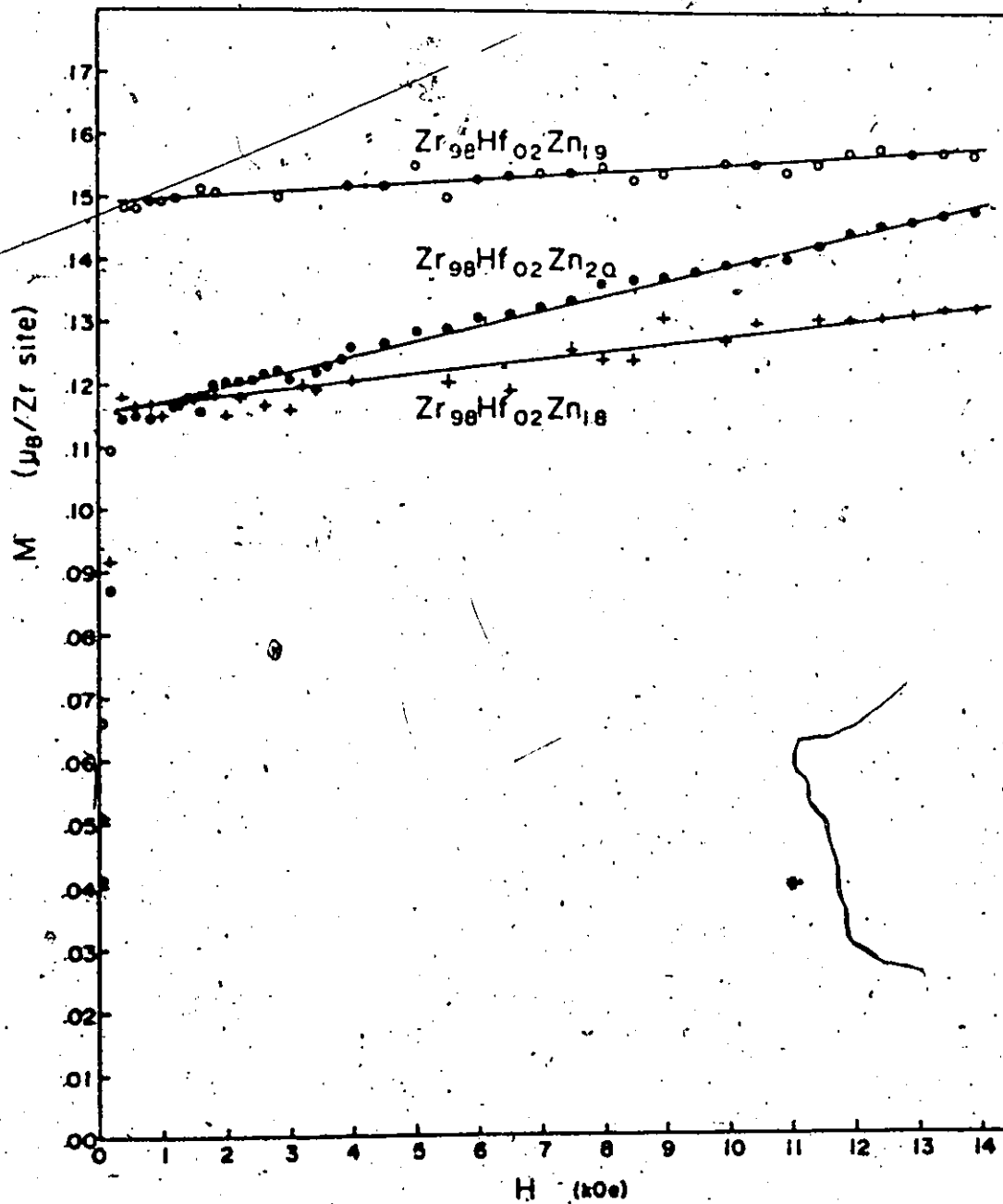


Figure 4-4

The Measured Bulk Magnetization

for samples 14, 11, 4, 7, 12 and 5 (from the top
down).

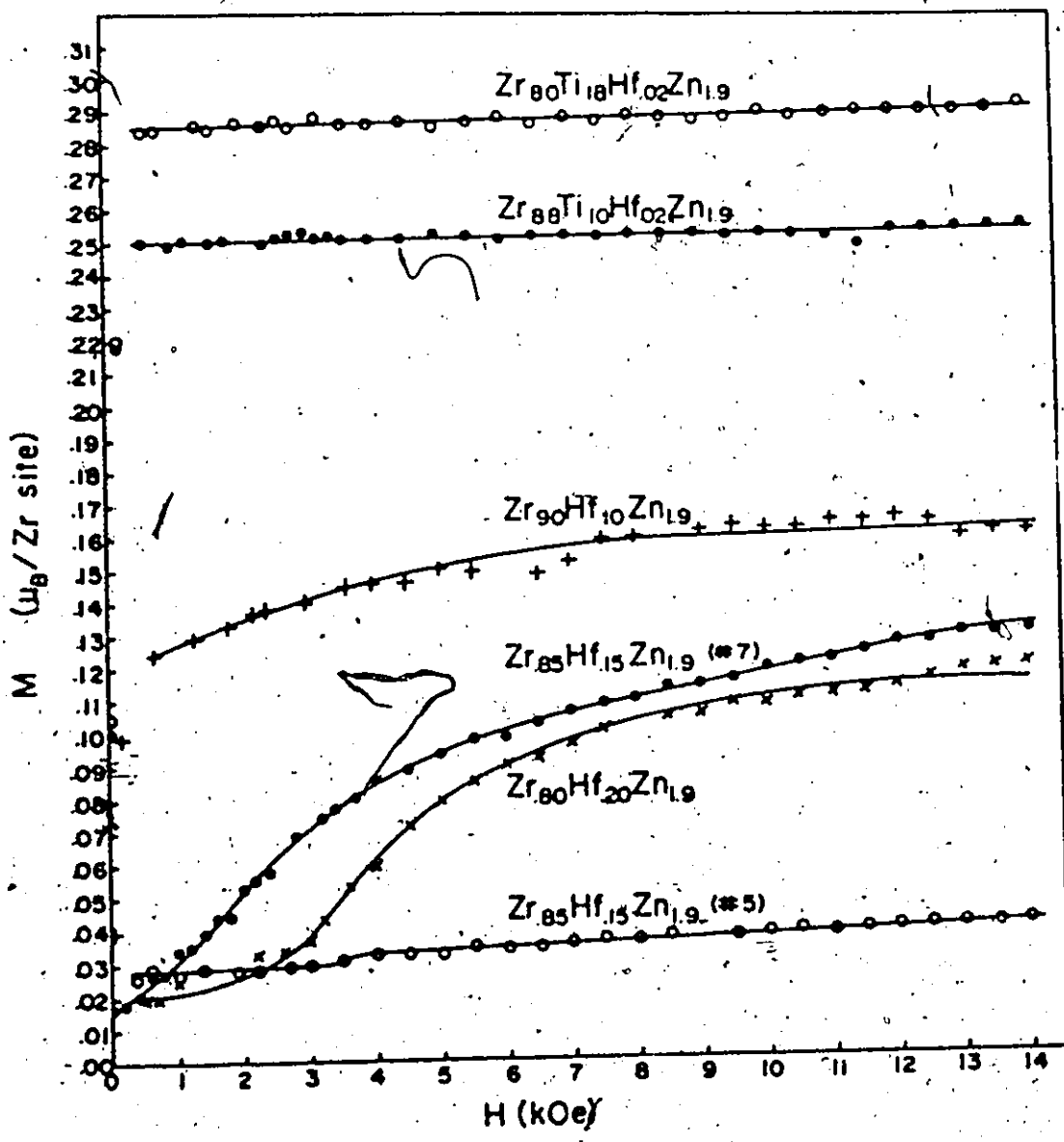


Figure V-5

$M^2(0,T)$ Plotted Against T^2

for samples 8, 10 and 1 (from the top down). The open circles are extrapolations from the M vs. H graph.

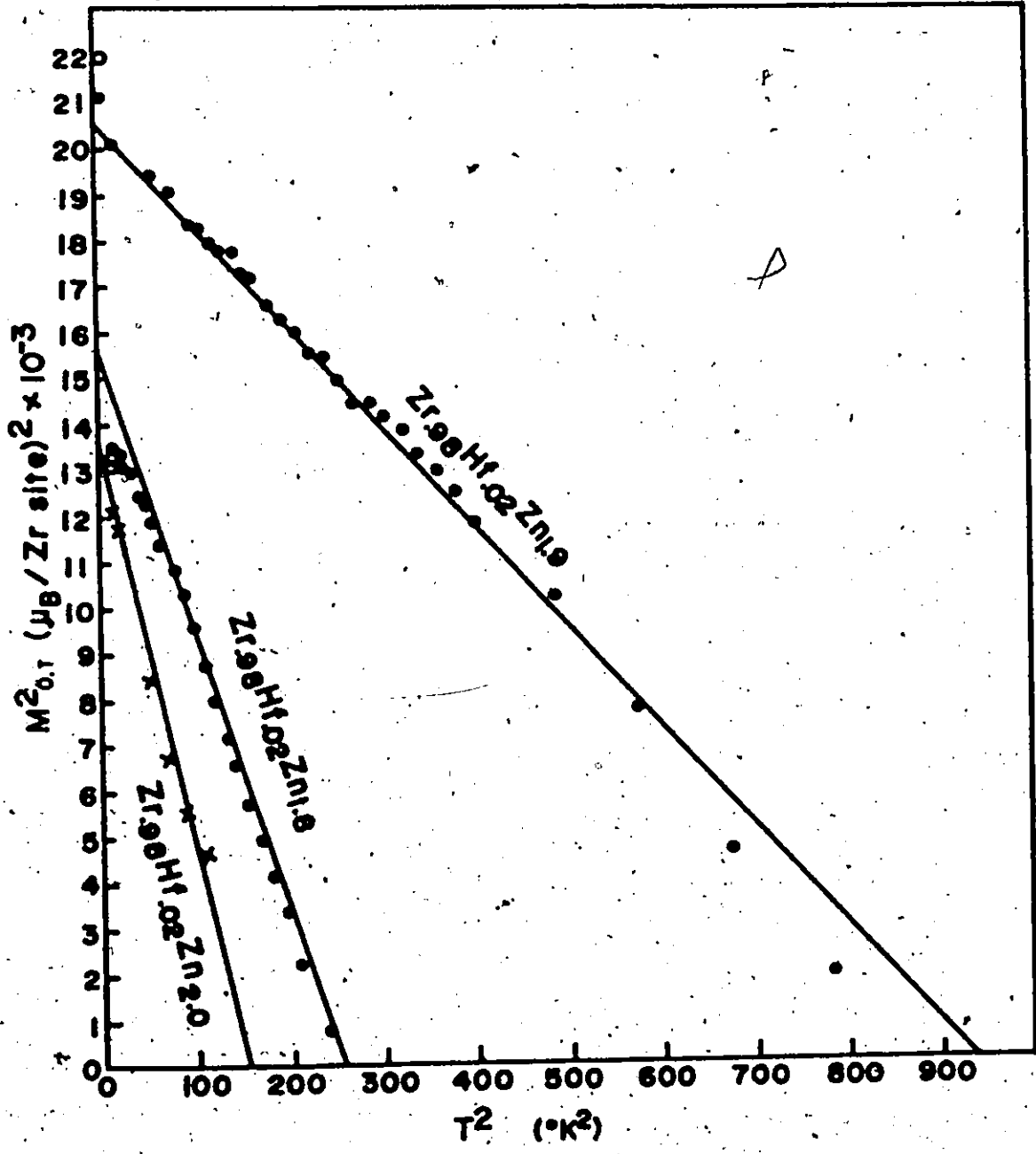
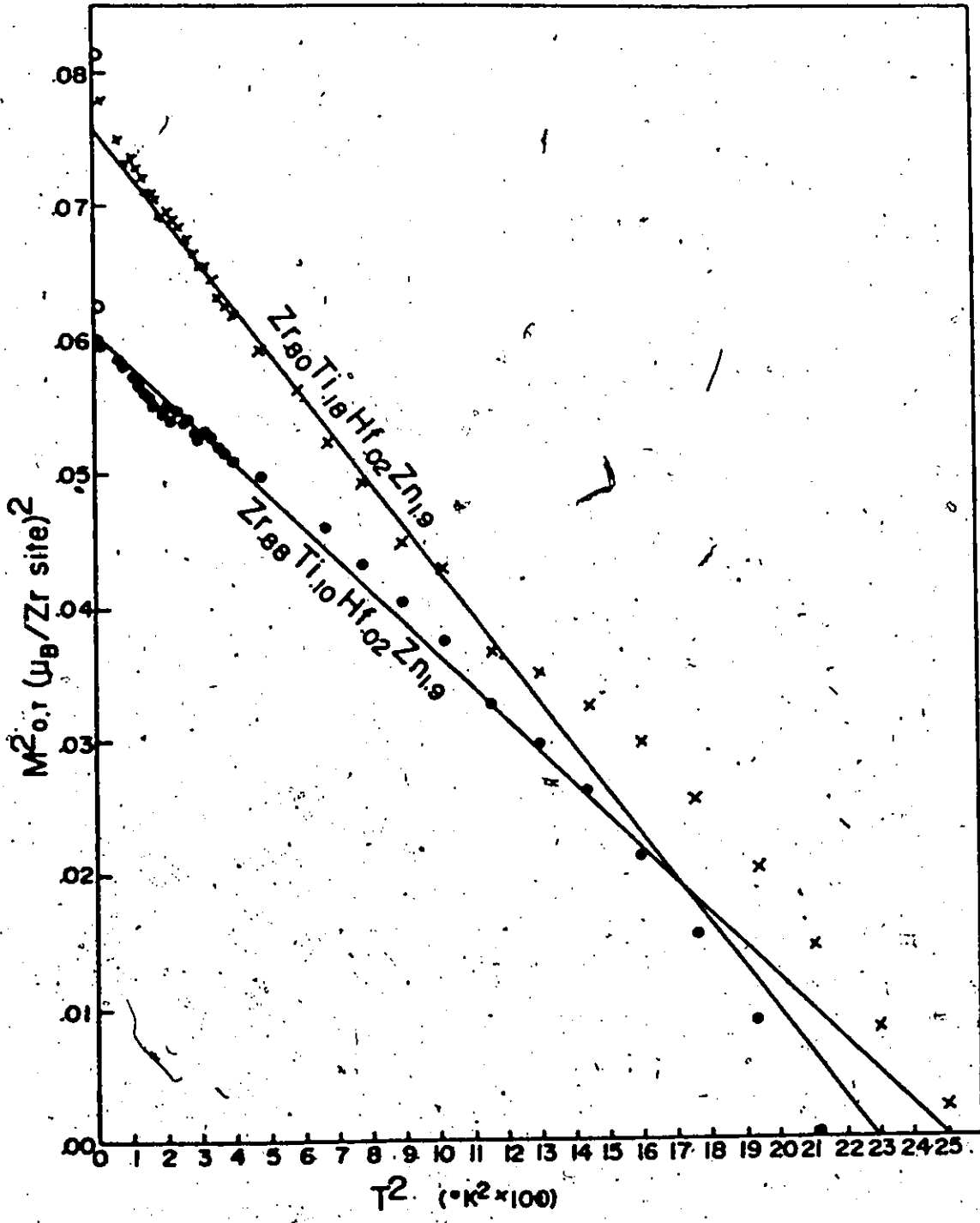




Figure V-6

$M^2(O,T)$ Plotted Against T^2

for samples 14 and 11 (from the top down). The open circles are extrapolations from the M vs. H graph.



site) is less than the magnetization for the magnetic part alone.

Estimates of the magnetic fraction have already been made from the neutron activation and X-ray analyses. Ogawa has found that, to a good approximation the magnetization is proportional to $T_c M(0,0) = .002 T_c$.

So yet another estimate of the magnetic fraction in each sample is tabulated in Table VI-3. The three different estimates are weighted by their variances to arrive at the best value. The corrected values of $M(300, H)$ are entered in Table VI-1 to be compared with the hyperfine fields (which were measured at that field and temperature).

They are also compared graphically. (Fig. VI-5).

A large fraction of most of the samples has been found to be non-magnetic. Probably the biggest factor contributing to the poor sample quality was the small volume of the pellets made. This was felt to be necessary for safety, to avoid high radiation fields. In this case they were about 10 mR/hr at a distance of an inch. High specific activity was needed for counting because of the small size of the source cavity in the magnet.

TABLE V-2 MEASURED FEASIBILITY OF GUN ENRICHMENT

SAMPLE NO.	NOMINAL COMPOSITION	UNCORRECTED (W_{235}/W_{238})	T_c (%)	ACTIVATION	X-RAY	MEASURED FEASIBILITY
1	Zr .96 Hf .02 Zn 2.0	$.12 \pm .02$	12.9 ± 2	$.76 \pm .06$	$.80 \pm .10$	$1.9 \pm .4$ $.77 \pm .06$
10	Zr .98 Hf .02 Zn 1.6	$.12 \pm .02$	10 ± 2	$.71$	$(.71)^*$	$1.2 \pm .4$ $.71 \pm .06$
18	Zr .98 Hf .02 Zn 1.9	$.14 \pm .02$	30 ± 2	$.92$	$.87$	$.72 \pm .20$ $.96 \pm .06$
4	Zr .90 Hf .10 Zn 1.9	$.09 \pm .02$	8 ± 2	$.67$	$.87$	$1.2 \pm .2$ $.87 \pm .06$
7	Zr .85 Hf .15 Zn 1.9	_____	_____	$.91$	$.92$	_____
5	Zr .85 Hf .15 Zn 1.9	_____	_____	$.57$	$.35$	_____
12	Zr .80 Hf .20 Zn 1.9	_____	_____	$.89$	$.95$	_____
11	Zr .89 Hf .10 Zn 1.9	$.25 \pm .03$	50 ± 2	$.77$	$.65$	$.62 \pm .10$ $.79 \pm .06$
14	Zr .80 Hf .16 Zn 1.9	$.28 \pm .03$	48 ± 2	$.75$	$.90$	$.64 \pm .10$ $.81 \pm .06$

*The numbers for this column were normalized to the neutron activation number for sample 10.

CHAPTER VI

DATA ANALYSIS AND EXPERIMENTAL RESULTS

1. DATA ANALYSIS

The time dependence of the gamma ray coincidences has the form:

$$W(\theta, H, t) = [1 + b_2 \cos 2(\theta - \omega_L t) + b_4 \cos 4(\theta - \omega_L t)] \exp(-t/\tau),$$

where θ is the angle between counters, H is the field acting on the nuclei, τ is the mean lifetime of the 482 keV state and ω_L is the Larmor precession frequency. In these experiments $b_2 = -0.91$ and $b_4 = -0.02$.

Figure VI-1 illustrates the detector configuration used for the correlation experiments in this thesis. Also depicted is the relative intensity of the 482 keV gamma rays detected by the counters at $+135^\circ$ and -135° . As the correlation pattern rotates, the intensity, besides decreasing exponentially, varies sinusoidally with a phase difference of π between the two detectors. Figure VI-2 shows the two time spectra for ferromagnetic ^{60}Co at 1.9 kOe with an external polarizing field of 3 kOe.

After background subtraction, the function:

$$R(t) = \frac{W(+135^\circ) - W(-135^\circ)}{W(+135^\circ) + W(-135^\circ)} \quad (\text{VI-1})$$

was calculated. The corresponding theoretical function is:

$$R(t) = \frac{b_2 \sin 2\omega_L t}{1 - b_4 \cos 4\omega_L t} = b_2 \sin 2\omega_L t \quad (\text{VI-2})$$

Figure VI-1

Detector Configuration and Angular Correlation Pattern

The diagram illustrates how, as the angular correlation rotates, the gamma ray intensity varies periodically but with opposite phase for the detectors at $+135^\circ$ (counter 1) and -135° (counter 2).

The direction of rotation is clockwise for a magnetic field pointing out of the paper and a positive g factor.

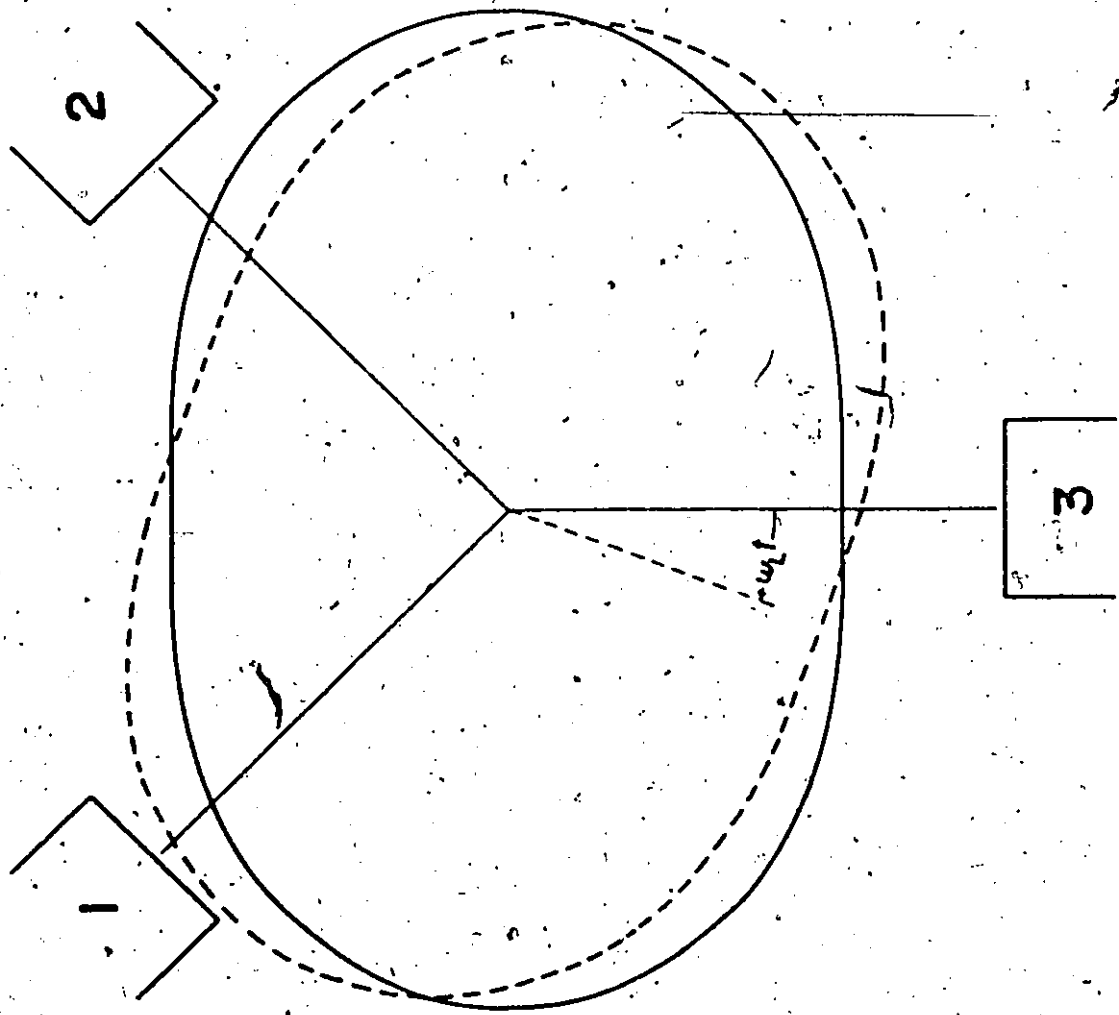


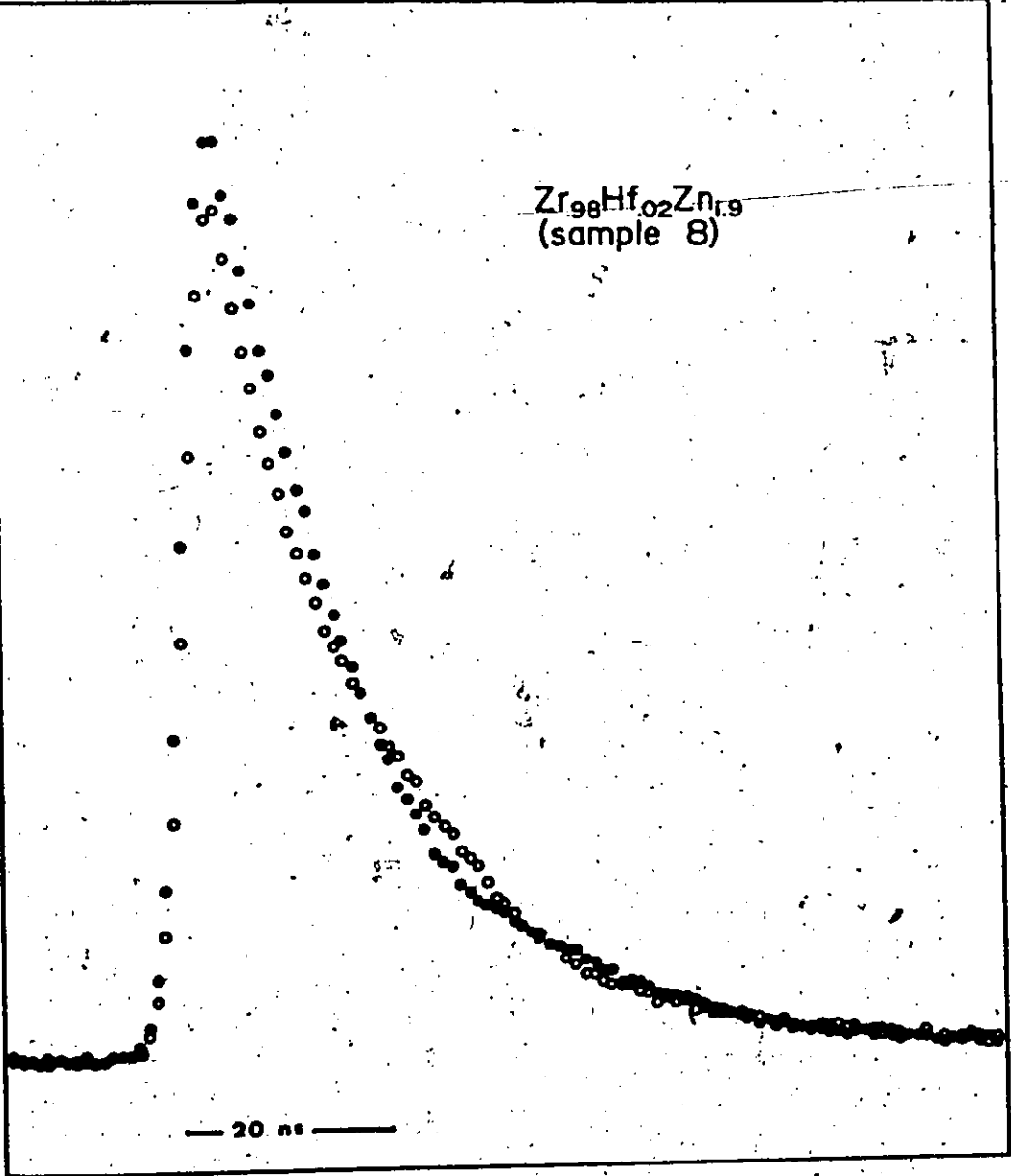
Figure VI-2

An Example of the Untreated Data

These are the time spectra collected for coincidences between detectors 1 and 3 - dark circles, and for coincidences between detectors 2 and 3 - open circles. (see Fig. VI-1).

COUNTS

$Zr_{98}Hf_{02}Zn_{1.9}$
(sample 8)



— 20 ns —

TIME

The measurements were also made with the detectors interchanged so that $R(t)$ could be calculated separately for each detector. Because of the finite time resolution (1.6 ns), $t = 0$ is about half-way up the steeply rising edge of the time spectrum. The function $R(t)$ makes information in this region much more easily accessible than from a single spectrum. Oscillations from quadrupole interactions have the same phase at 135° and -135° so that their effect would largely cancel in $R(t)$. No quadrupole oscillations were noticeable, however, in the single spectra.

Figure VI-3 shows the function $R(t)$ at 300°K (a) and at 4°K (b) for $\text{Er}_{0.98}\text{Ta}_{0.02}\text{In}_{1.9}$. The function $R(t)$ has been fitted by the method of non-linear least squares. Since the upper curve was measured above the Curie temperature, the only contribution to the effective field at the nucleus is from the external field. The difference in phase between the two curves indicates that the hyperfine magnetic field for ^{181}Ta in ErIn_2 is negative. The amplitude at both temperatures is only a third of the theoretical value of b_2 which is -0.21 .

The effective field is related to the Larmor precession frequency by:

$$\omega_L = -\gamma_n H_{\text{eff}} \quad \text{(III-2)}$$

The g factor of the 482 keV level of ^{181}Ta is 1.32 ± 0.01 . H_{eff} (from curve (b) of Fig. VI-3) was determined to be -14.5 ± 0.2 kOe.

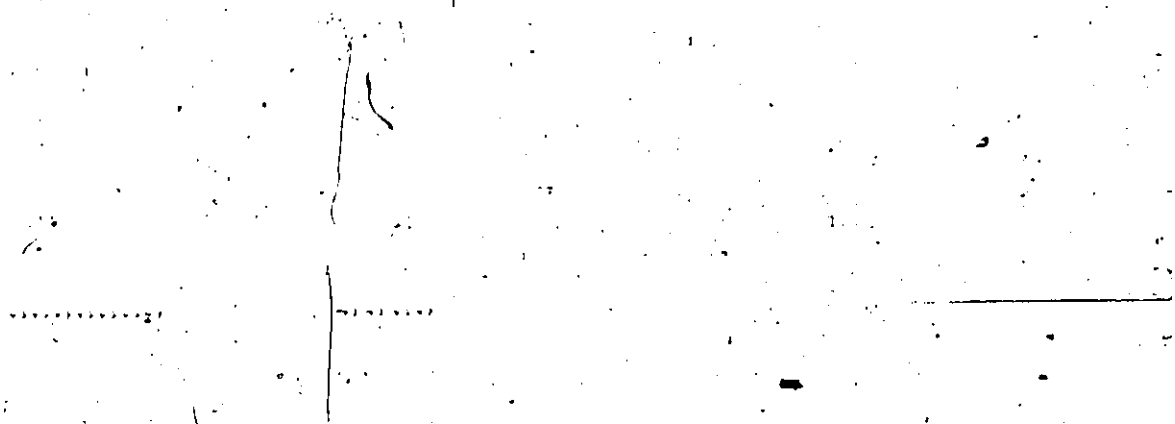
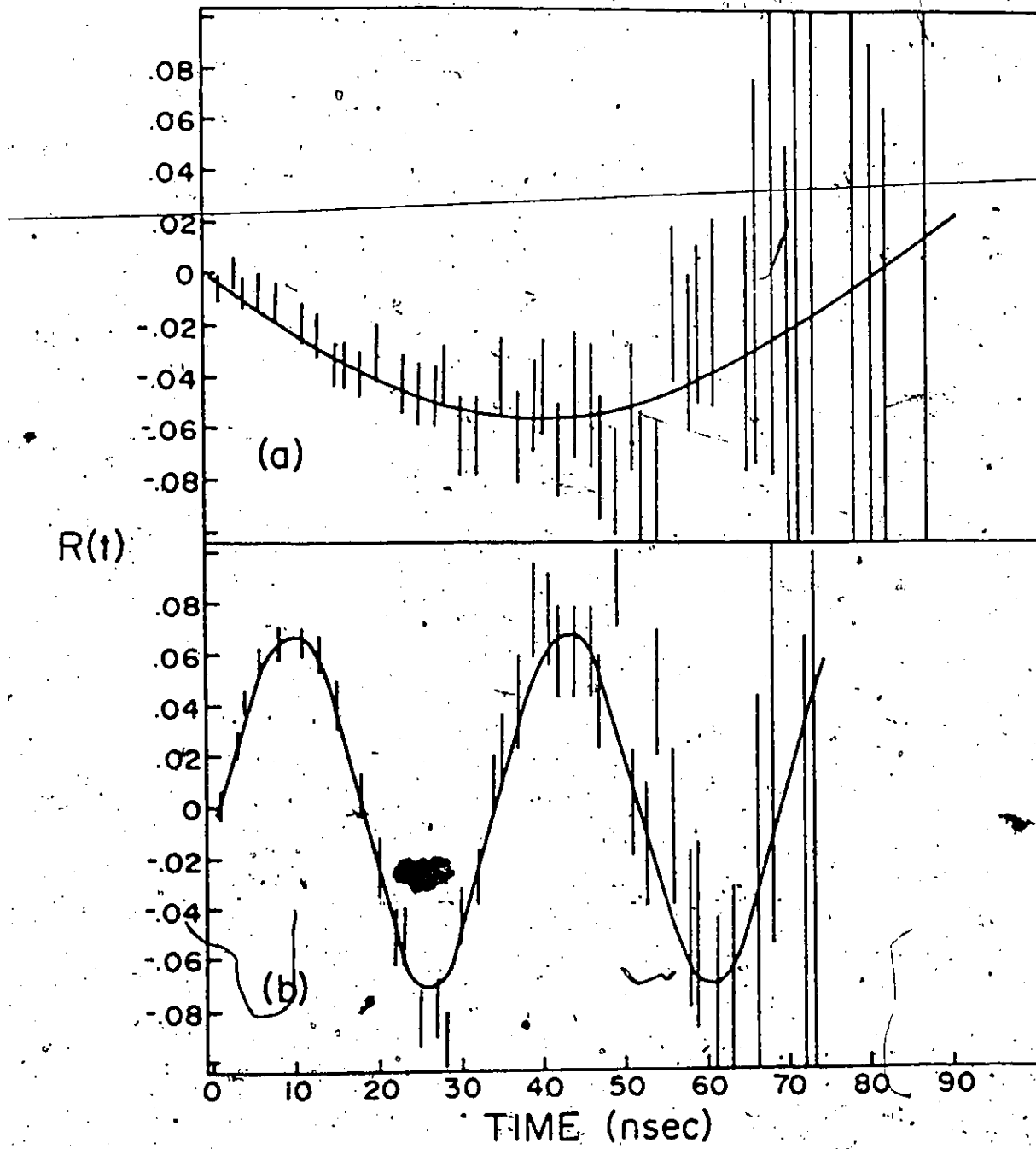


Figure VI-3

The Function $R(t)$ and Least Squares Fit

These curves are for sample 8 at (a) 300°K and (b) 320°K.

Curve (b) is for the data shown in Figure VI-2.



The hyperfine field is given by:

$$H_{hf} = H_{eff} - (H_{ext} + \frac{4}{3}\pi M - D_4\pi M) \quad (II-6)$$

The magnetization measured for the sample was $4\pi M(4^\circ K, 3 \text{ kOe}) = 1.5 \text{ kOe}$ and the demagnetizing factor is 0.46. The external field was $+3.0 \pm 0.1 \text{ kOe}$.

From Eqn. II-6 the hyperfine field experienced by ^{181}Ta nuclei in $\text{ZrZn}_{1.9}$ is:

$$H_{hf} = -17.3 \pm 0.3 \text{ kOe.}$$

2. BACKGROUND SUBTRACTION

In a typical experiment, the 133 keV gamma detector was about 4.5 cm from the source with 1/32" of cadmium absorber for low energy X-rays. The 482 keV detectors were about 3.5 cm from the source and had 1/8" of lead absorber to cut down the intensity of 133 keV gammas. Typical count rates were 5000/sec for 482 keV, 10000/sec for 133 keV and about 30 coincidences/sec. Sometimes, after the TAC has been started by a 133 keV gamma, a 482 keV gamma is detected which is from a different nucleus. This situation is called a chance coincidence (as opposed to a true coincidence) and the second gamma ray is uncorrelated in time with the first. (In practice, the TAC is actually started by the 482 keV gamma and stopped by the artificially delayed 133 keV in order to decrease the dead time of the TAC). Chance coincidences result in background which decreases approximately as $\exp(-\lambda_c t)$ where λ_c is the probability of chance coincidence per unit time. If the probability

of a chance coincidence in the time of a TAC cycle (200 ns) is small, the exponential becomes approximately linear or, for a very low probability, nearly constant. For the count rate stated for stop pulses (10000/sec), $\lambda_c = 10^{-5} \text{ ns}^{-1}$ so that the fractional decrease in background in 200 ns is only 2×10^{-3} .

Before the function $R(t)$ (Eqn. VI-1) can be calculated, the background must be subtracted from the time spectra. This was done by eye on the PDP 11/05 computer. An exponential curve with adjustable decay constant and amplitude was displayed along with the data. When the data coincided with the curve, background subtraction was stopped. This always occurred as the background before the $t = 0$ edge of the spectrum became zero, showing that it was justifiable to subtract a constant background. Typically, there were about 50000 counts collected in the peak channel and 500 background counts per channel. The background could be determined within about 10 counts per channel. Least squares fits could have done better but it would have made no detectable difference in $R(t)$.

3. STATISTICAL ERROR

The variance σ_p^2 for each data point (or peak area) after background subtraction is given by:

$$\sigma_p^2 = P + B + (\Delta B)^2$$

where P is the number of counts after background subtraction, B is the background subtracted and ΔB is the uncertainty in how well the background is known.

If a sample S of constant background is taken in order to remove background B from data (P+B), then the variance in the calculated peak area P is:

$$\sigma_p^2 = (P+B) + B^2/S$$

The smallest variance possible is then:

$$\sigma_p^2 \text{ min} = (P+B)$$

and not P+2B as it is often argued. This is because the background under a peak is statistically correlated with the data before background subtraction. To demonstrate this, suppose that data T is measured and also the true average background \bar{B} under the peak is calculated (from a large sample say).

Then the best choice of P is:

$$P = T - \bar{B}$$

Its deviation from the true value \bar{P} is:

$$P - \bar{P} = T - (\bar{P} + \bar{B}) = T - \bar{T}$$

which has a Poisson distribution with variance:

$$\sigma_p^2 = \bar{T}$$

The best estimate of \bar{T} is T. The r.m.s. deviation of T from \bar{T} is \sqrt{T} so that the relative error is $1/\sqrt{T}$. When T is large then,

$$\sigma_p^2 = T$$

is a good approximation.

From the variances σ_p^2 in the spectra, the variances σ_R^2 for each point of the function R(t) are calculated. In the least squares fit to R(t),

the points are weighted by $1/\sigma_R^2$. The standard deviation of each parameter was taken to be the square root of the corresponding diagonal element of the error matrix (inverse of the curvature matrix) which was generated by the least squares program.

4. EXPERIMENTAL RESULTS

Figs. VI-3 and VI-4 summarize graphically the effective field measurements at ^{181}Ta nuclei. The largest χ^2 was 1.7 for sample 12. All others were less than 1.4. The room temperature measurement shown in Fig. VI-3 is typical of those made using the other samples. In all cases, the amplitude was approximately the same as the amplitude at 4°K. (Both are only a third or less of the theoretical amplitude). Table VI-1 and Fig. VI-5 present the hyperfine fields calculated from the effective field using Eqn. II-6 and the magnetization data at the same temperature and external field. The relative size of the scales on the graph is somewhat arbitrary. The way which was chosen approximately minimizes the differences between the two sets of data. If the data had instead been normalized at $^{98}\text{Zr}_{.02}\text{Hf}_{.98}\text{Zn}_{1.9}$, the situation would not change much.

If the uncorrected magnetizations had been plotted in Fig. VI-5, the main tendencies do not change much for hafnium. The magnetization and hyperfine field vary in the same manner until after 10% Hf. The magnetization drops quickly after that ($M(0,0)$ drops to zero by 15%) in agreement with the results of Ogawa. The hyperfine field remains high even until 15% Hf.

Figure VI-4

The Function $R(t)$ and Least Squares Fit

at 4°K for samples:

1. $Zr_{.98}Hf_{.02}Zn_{2.0}$
10. $Zr_{.98}Hf_{.02}Zn_{1.8}$
4. $Zr_{.90}Hf_{.10}Zn_{1.9}$
12. $Zr_{.80}Hf_{.20}Zn_{1.9}$
5. $Zr_{.85}Hf_{.15}Zn_{1.9}$
7. $Zr_{.85}Hf_{.15}Zn_{1.9}$
11. $Zr_{.88}Ti_{.10}Hf_{.02}Zn_{1.9}$
14. $Zr_{.80}Ti_{.18}Hf_{.02}Zn_{1.9}$

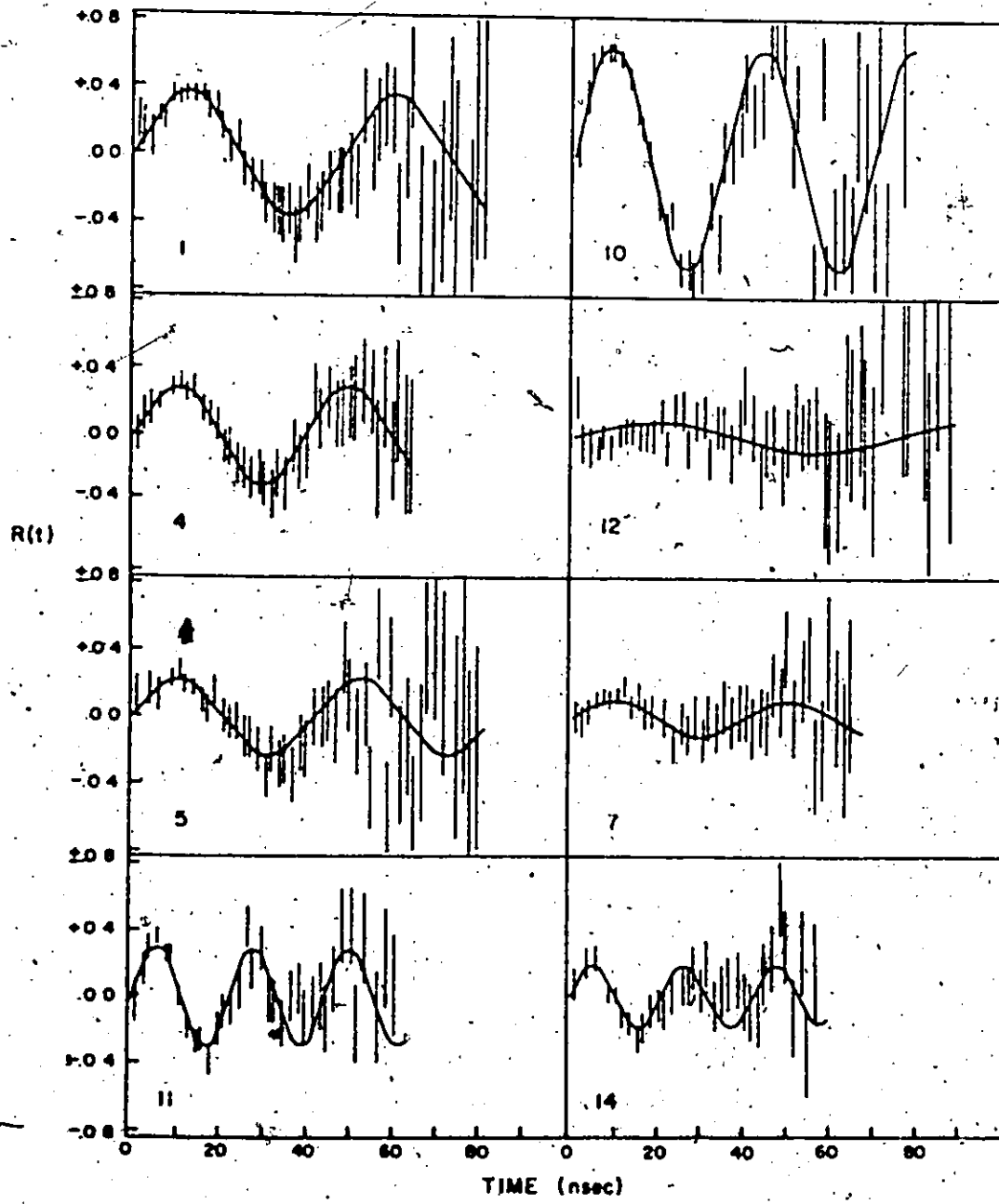


TABLE VI-1 NMR MAGNETIZATION AND HYPERFINE FIELDS

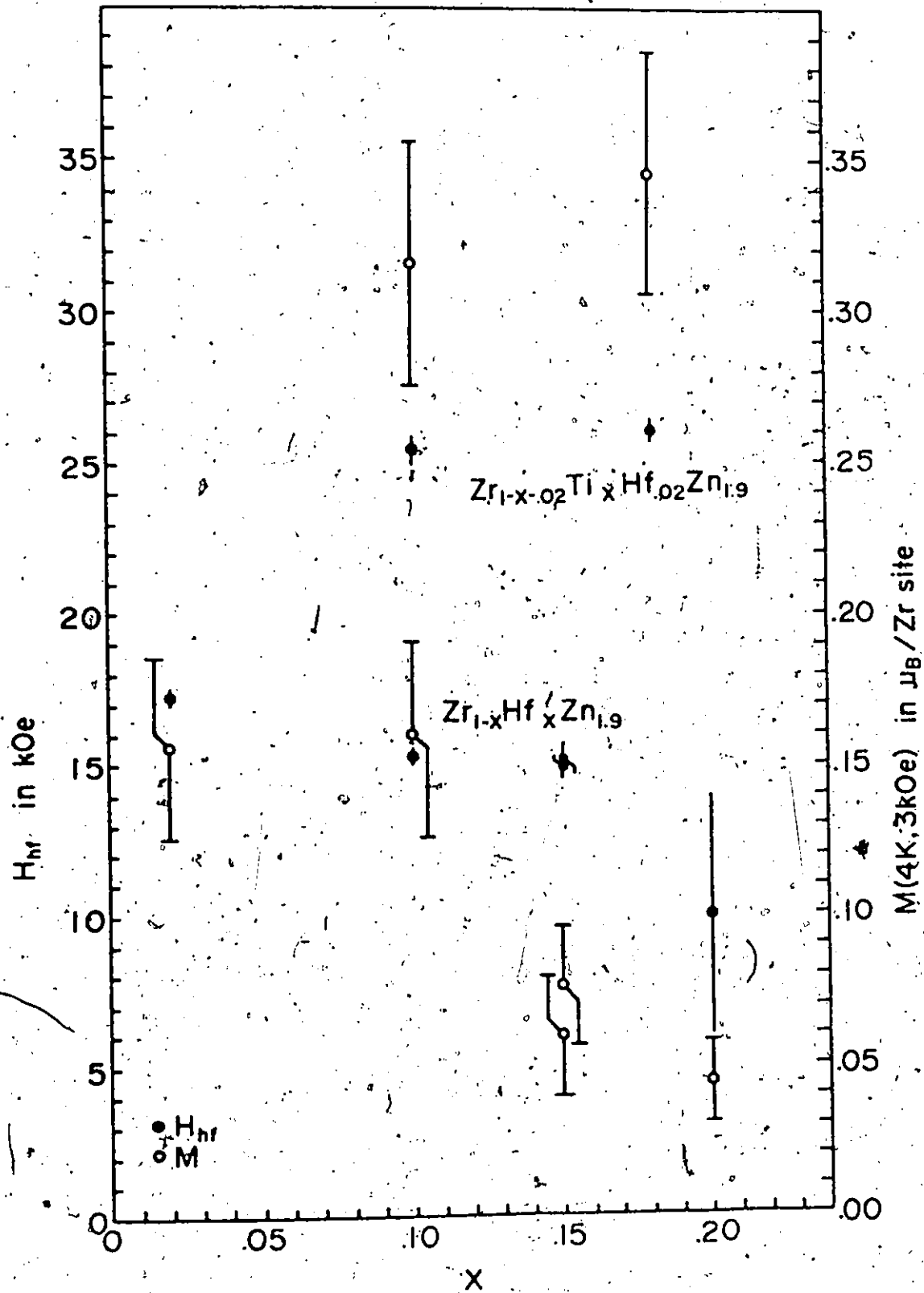
SAMPLE NO.	NOMINAL COMPOSITION	T _c (°K)	UNCORRECTED		CORRECTED		h _{hf} (kOe)	h _{eff} (kOe)	h _{hf} (kOe)
			H (kOe)	(μ _B /Zr)	H (kOe)	(μ _B /Zr)			
1	Zr .98 Hf .02 Zn 2.0	12.5 ± 2	.12 ± .02	.156 ± .040	1.6	-10.3 ± .3	-13.1 ± .4		
10	Zr .98 Hf .02 Zn 1.8	16 ± 2	.12 ± .02	.169 ± .040	1.7	-13.6 ± .3	-16.4 ± .4		
8	Zr .98 Hf .02 Zn 1.9	30 ± 2	.15 ± .02	.156 ± .030	1.6	-14.5 ± .2	-17.3 ± .3		
4	Zr .90 Hf .10 Zn 1.9	8 ± 2	.14 ± .02	.161 ± .030	1.6	-12.5 ± .2	-15.3 ± .3		
7	Zr .85 Hf .15 Zn 1.9	—	.07 ± .01	.077 ± .020	.8	-12.3 ± .4	-15.2 ± .5		
5	Zr .85 Hf .15 Zn 1.9	—	.03 ± .01	.060 ± .020	.6	-11.9 ± .3	-14.8 ± .4		
12	Zr .80 Hf .20 Zn 1.9	—	.04 ± .01	.045 ± .015	.5	-7 ± 4	-10 ± 4		
11	Zr .86 Ti .10 Hf .02 Zn 1.9	50 ± 2	.25 ± .03	.316 ± .04	3.2	-22.8 ± .3	-25.4 ± .4		
14	Zr .80 Ti .18 Hf .02 Zn 1.9	48 ± 2	.28 ± .03	.346 ± .04	3.5	-23.5 ± .3	-26.1 ± .4		

$$H_{hf} = H_{eff} - (3.0 \pm 1.) + (.46 \frac{1}{3}) 4 \mu_B \quad (\text{Eqn. II-6})$$

Figure VI-5

The Hyperfine Fields (Dark Circles) and Corrected Bulk Magnetizations

at 4°K and 3 kOe (open circles), plotted as a function of impurity concentration. The two higher sets of points are for titanium impurity; the remaining ones, for hafnium impurity.



For titanium impurity, when the uncorrected magnetization is plotted, the points are consistent with the hyperfine field but the hyperfine fields are lower for both 10% Ti and 18% Ti. For the corrected magnetization which is plotted, the points are increased so that the error bars no longer overlap even though they are larger. That is, the fractional increase in magnetization is greater than the fractional increase in hyperfine field. The hyperfine fields change by at most 0.1 kOe as a result of the magnetization correction. The hyperfine field for sample 1 is inconsistent with the other two measurements for 2% Hf but this sample was made at 916°C. As discussed in Chapter V (Section 2), the magnetic properties for samples made at high temperatures are not reproducible (although samples 5 and 7 are consistent).

CHAPTER VII

DISCUSSION OF THE RESULTS AND INTERPRETATION

There are four aspects of the results that will be discussed in this chapter. The first is the discrepancy between the observed and theoretical amplitude of the oscillations in the TDPAC experiments. The second aspect is the importance of the zinc concentration in the $ZrZn_2$ phase. The third section is about the size of the hyperfine field measured and its comparison with the prediction of a model. The last thing to be considered is the impurity concentration dependence of the hyperfine field. The results indicate that the hyperfine field does not follow the magnetization as the impurity concentration increases.

1. THE AMPLITUDE OF THE OSCILLATIONS

The amplitude of the oscillations observed in the TDPAC experiments (Figs. VI-3 and VI-4) was never more than about a third of the theoretical value. The reason for this is not just that most of the atoms are in non-magnetic parts of the sample. If this were the case, then the amplitude at room temperature would be large. In fact it is not noticeably larger than at 4 degrees. At least two thirds of the ^{181}Ta nuclei are not contributing to the oscillations in the angular correlation. The only satisfactory explanation seems to be that the nuclei are experiencing large electric field gradients, producing quadrupole oscillations too high in frequency (say above

200 MHz) to be resolved by the apparatus. Using equations III-3 and III-4 and taking into account the Sternheimer anti-shielding factor (section II-5b), this corresponds to a field gradient in excess of 4×10^{16} V/cm² (before amplification).

If hafnium tended to clump together in the sample or to oxidize, the quadrupole frequencies should be clearly distinguishable (especially in sample 12 with 20% Hf) in the time spectra obtained. The field gradients might be caused by strains (Blythe) in the ZrZn₂ or by large amounts of hafnium trapped at grain boundaries. The latter is a likely possibility in view of the coarse texture of the samples.

Small oscillations are not peculiar to measurements in ZrZn₂ but have been reported by many other researchers on a variety of different magnetic systems (Cameron et al., Keszthelyi et al., Agarwal et al., Oddou et al.). The problem points out a major advantage of TDPAC over methods (like time-integral PAC or nuclear orientation) which measure the average hyperfine field on all the probe nuclei. These methods would obtain values several times too small if they could be measured at all. In the time-differential method, however, only the nuclei experiencing a field contribute to the effect observed.

2. ZINC CONCENTRATION IN THE ZrZn₂ SAMPLES

The reason for making three samples all with different zinc concentrations (samples 1,8,10) was originally to see whether or not there was a maximum in the hyperfine field at ZrZn_{1.9} as there is for

the magnetization. As already mentioned in section V-1, the findings of Knapp et al., indicate that the cubic Laves phase occurs only at this composition when the samples are made at 700°C., thus insuring their reproducibility. The hyperfine field measured for sample 1 is the only indication in the results in this thesis, that the zinc concentration has any effect on the $ZrZn_2$ phase. It was made at 916°C.

At first glance, it appears that for samples made at high temperatures, the change in magnetization with zinc concentration might be explained by the change in the Fermi level when zinc atoms add electrons to the s-p band as the concentration increases. If a zinc atom were to contribute two electrons, the shift in the Fermi level would be about the same as the width of the narrow d band of $ZrZn_2$. This explanation is not valid because the zinc atoms do not contribute enough electrons.

The band calculations of D.L. Johnson and of Koelling et al. (KJKH) completely neglect the presence of zinc atoms and deal only with zirconium atoms on a diamond lattice. Johnson considers this to be equivalent to $ZrZn_{1.9}$. He states, "While the Fermi level may be slightly raised upon adding in the zinc atoms, it will certainly not be raised by two electrons per zinc atom, as this would cause a severe charge imbalance, and it (the Fermi level) could conceivably be lowered relative to the Zr d complex." In view of their band calculations, an increase in the Fermi level would quickly make the crystal structure unstable. The d electrons of the zinc do not mix into the

zirconium d band appreciably because they are approximately 10 eV lower in energy and so no moment should be expected to form. This is supported by the measurement by Mishiara et al. of the low hyperfine field at iron substituting at the zinc site (3 ± 1 kOe) and by the low spin density near the zinc reported by Shirane et al. who used diffuse neutron scattering.

The relative stability and optimum magnetic properties of $ZrZn_{1.9}$ appear to result from the large size of the zinc atoms. Departure from that concentration of zinc could be expected to produce strains in the lattice. Samples made at low temperatures would be less likely to contain excess zinc forced into the lattice than those made at higher temperatures.

The conclusion is that, after the magnetization correction (because not all of the sample is in the magnetic $ZrZn_2$ phase), the points plotted in Fig. VI-5 show the behaviour of the magnetization as a function of hafnium and titanium concentrations only. The behaviour is neither a result of the manner of sample preparation (or poor quality), nor of differences in zinc concentrations.

3. THE MAGNITUDE AND SIGN OF THE HYPERFINE FIELD

Most, but not all of the hyperfine fields measured so far in magnetic materials have been negative - that is, opposite in direction to the applied field. It could not be certain ahead of time that the hyperfine field at ^{181}Ta in $ZrZn_2$ would be negative. The value measured was -17.3 ± 0.3 kOe for $_{98}\text{Hf}_{0.02}\text{Zn}_{1.9}$. The decrease in

hyperfine field with hafnium concentration is linear up to 15% Hf and the percentage decrease is the same as the percentage of hafnium impurity. The hyperfine field at a single tantalum nucleus in pure $ZrZn_2$ should be about 2% higher than the value measured.

The behaviour of the magnetization is the same but only to 10% hafnium so, at least in low concentrations, hafnium atoms (and presumably tantalum atoms also) behave like a diamagnetic impurity. This has been found to be true for tantalum in nickel (Barrett et al.).

A crude model for hyperfine magnetic fields at diamagnetic impurities (those which have no localized moment) in iron, cobalt and nickel has been used by Shirley et al. This is the conduction electron polarization or CEP model. The conduction s electrons of the magnetic host have a positive polarization within the host atom but are negatively polarized outside the d shell. The impurity atom is treated as if it were free and the polarized s electrons in the conduction band as if they were the outer valence electrons of the impurity. The net polarization of the electrons is assumed to be proportional to the host moment. The hyperfine field is predicted by:

$$H_{hf} = 0.027 \mu H_{ns} \quad (\text{VII-1a})$$

where μ is the host moment and H_{ns} is the hyperfine field that would be produced in a free impurity atom by a single atomic ns electron. The constant 0.027 was obtained by fitting the hyperfine fields for 17 cases of impurities in iron, cobalt and nickel hosts. They found that, "the average deviation is only 2 kG and the r.m.s. magnitude

of the deviation is 54 kG in a quantity of average magnitude 260 kG." Because of fitting, factors other than CEP may have been absorbed by the parameter (core polarization for example). For tantalum, H_{6s} has been calculated to be -8300 kOe so that the hyperfine field is given by:

$$H_{hf} = -224\mu \quad (\text{VII-1b})$$

The hyperfine fields have been plotted for tantalum in iron, nickel and $ZrZn_2$ in Fig. VII-1. The model overestimates the magnitude of the field by a factor of two. The constant in equation VII-1 should not be expected to be the same for $ZrZn_2$ as for the iron series hosts. If a horizontal line were to be drawn through nickel, to which band models apply better than the other elements of the 3d group, then the agreement becomes much better (23 kOe). In $ZrZn_2$ there is a maximum in the unpaired spin density mid-way between zirconium sites. This might possibly contribute some positive CEP which would lower the constant in equation VII-1.

4. IMPURITY CONCENTRATION DEPENDENCE OF THE HYPERFINE FIELD

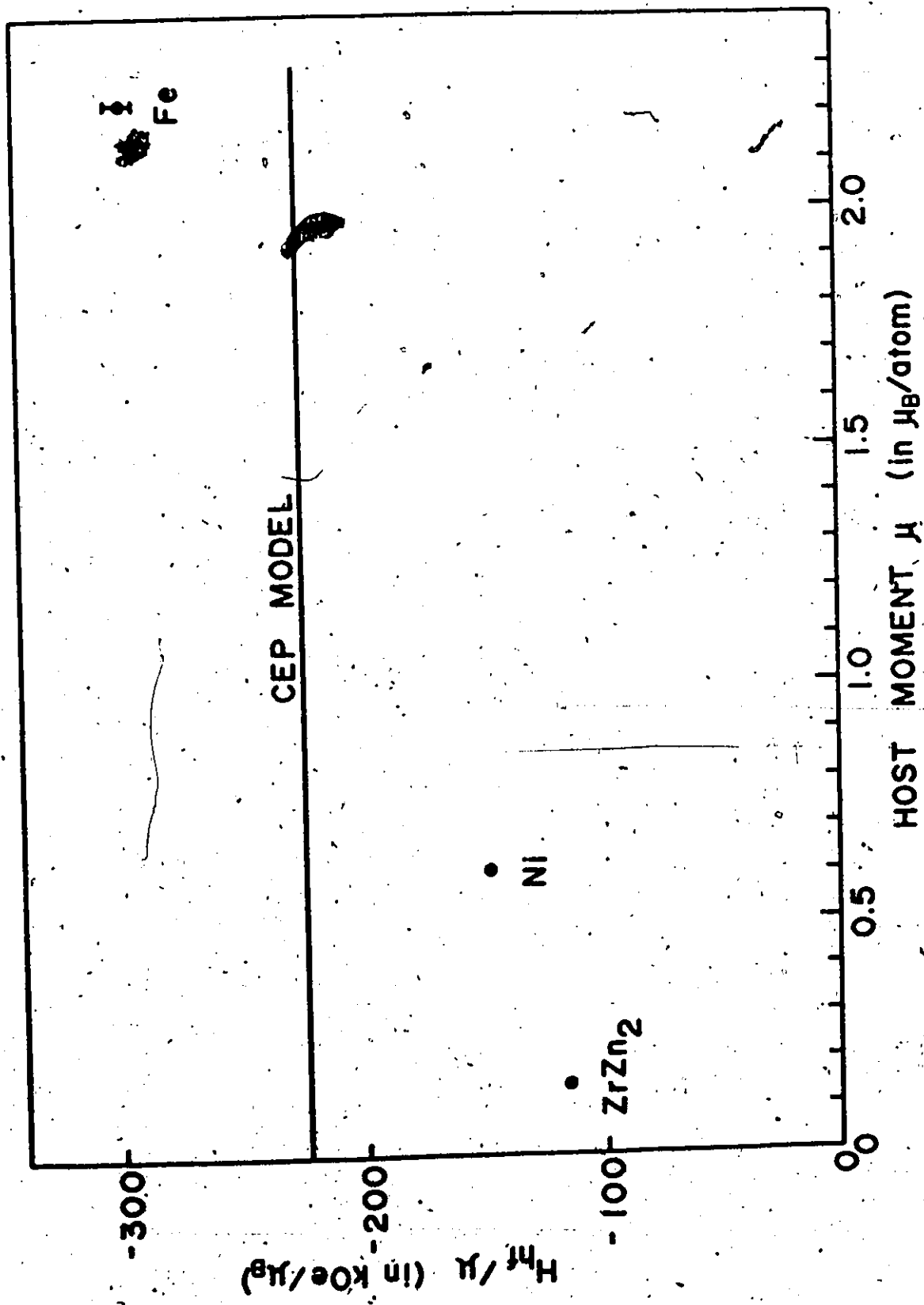
While the magnetization begins to drop at about 10% hafnium, the hyperfine field remains high until after 15%. For titanium impurity, on the other hand, the hyperfine field does not increase by as great a fraction as does the magnetization.

A possible explanation of the hafnium data is that, as the hafnium concentration increases, the proportion of sites which have all zirconium nearest neighbours (about half at 15% if the hafnium

Figure VII-1

The Conduction Electron Polarization (CEP) Model

for the hyperfine field at Ta in 3d ferromagnets. The point for $ZrZn_2$ is also plotted.



is randomly distributed) and the magnetization decreases. The actual decrease is faster than this crude approximation predicts. The tantalum nuclei that have all zirconium neighbours might still experience a high hyperfine field, while others that have one or more hafnium neighbours detect a lower field or possibly the external field.

The same type of explanation might also apply to the titanium data. The tantalum sites which had any titanium neighbours might be incapable of detecting a magnetic field (say because of large electric field gradients caused by the small size of the titanium atoms). The magnetization would increase around the titanium atoms but the probe nuclei capable of detecting a magnetic field would be at locations having less than the average magnetization.

These explanations may be totally incorrect. Possibly the reason for the observed effects is that the addition of impurity changes the distribution of unpaired spin density. Neutron scattering experiments could tell whether this is so.

A model with which the problem might be attacked is the coherent potential approximation (CPA), if the impurities do not distribute themselves in an ordered manner. Calculations of this complexity are, however, beyond the scope of this thesis.

APPENDIX

This appendix contains a listing of PROGRAM DIFCOR which was used for data acquisition and display and on-line analysis of the data acquired by a PDP 11/05 computer.

Because the count rate was low, data could be displayed and analyzed without stopping the acquisition. This allowed one to tell how an experiment was progressing. The fitting procedures were done on another computer.

Program DIFCOR acquires two spectra at a time in one of two memory locations, A or B. Location A was for detector 1 at $+135^\circ$ and detector 2 at -135° . Location B was for the detectors interchanged.

Location D was reserved for manipulating the spectra without altering the raw data in A or B. D consists of two spectra X and Y. X is a spectrum at $+135^\circ$ which has been moved from either A or B; Y is a spectrum at -135° from A or B. Either X or Y can be normalized to the other. (The spectra can be displayed superimposed, using switches on the display panel). The spectra can be shifted left or right and a constant background can be subtracted from either. X can be divided by Y and the quotient is stored in location W and displayed. Since the oscillations in X and Y are π out of phase, the oscillations in W have about twice the amplitude of the actual effect.

In order to see the oscillations in a single spectrum X, a pure exponential may be deposited in Y instead of another spectrum. The exponential can be fitted by eye, using switches on the display panel and computer console.

The spectra could be printed out or stored on paper tape.

PROGRAM DIFCOR

40=60

TO: 2TY
IR: 240
L=130
L0: ADCA
L2: 340
L=462

ADC ROUTING
2X 256 CHANNELS

ADCA: MOV ADC1, X0
BIT #157330, X0
INIE, OUT
BIT #23333, X0
INIE TWO
ASL X0
ADD C1, X0
ONE: INC(X0)
OUT: INC ADCSR
BTI
TWO: BIC #23333, X0
ASL X0
ADD C2, X0
BR ONE
ADCSR=164010
ADC1=164012
L=570

START: MOV #450, X6
DSPLY: CLR #164002
MOV #100, KSR
MOV C0, X5
LOOP: MOV (X5)+, #164004
INC #164000
INC #164002
CMP #164002, NC
BEQ HIGH
WAIT: TST #164000
BNE WAIT
BR LOOP
HIGH: MOV #164006, X5
BIC K4, X5
MOV X5, #164002
ASL X5
ADD C0, X5
MOV (X5), #164004
MOV #3, #164000
PAUSE: CMP #164000, K5
BNE PAUSE

DISPLAY

(Y REGISTER)
(Z REGISTER) INTENSITY
(X REGISTER)

INTENSIFY POINT

CLR #164000
 BR D9PLY
 C1: 10930
 C2: 11030
 C3: 10300
 NC: 2000
 LC: 14000
 DI: CLR #2
 M: CLR #2
 OP3: 14000
 OPL: 15300
 KA: 177000
 KS: 2
 .-1000

TTY: CMP TKB, #201
 EJE G02
 MOV #10330, C1
 MOV #11330, C2
 MOV #104, ADCSR
 RTI

G02: CMP TKB, #202
 EJE DISPA
 MOV #13000, C1
 MOV #12000, C2
 MOV #104, ADCSR
 RTI

DISPA: CMP TKB, #'A
 EJE DISPB
 CLR #164002
 MOV #10300, C0
 MOV #1000, NC
 MOV #12000, LC
 RTI

DISPB: CMP TKB, #'B
 EJE STOP
 CLR #164002
 MOV #12000, C0
 MOV #1000, NC
 MOV #14000, LC
 RTI

STOP: CMP TKB, #'S
 EJE DISPD
 MOV #4, ADCSR
 RTI

DISPD: CMP TKB, #'D
 EJE DISPX
 CLR #164002
 MOV #14000, C0
 MOV #1000, NC
 MOV #16000, LC
 RTI

ROUTING

FIRST ADDRESS FOR ADC DATA (BIT 13 CLEAR)
 FIRST ADDRESS FOR ADC DATA (BIT 13 SET)
 FIRST DISPLAY ADDRESS
 NUMBER OF CHANNELS DISPLAYED
 LAST +2 ADDRESS DISPLAYED
 2 MEANINGLESS INSTRUCTIONS
 (TO RESERVE THE LOCATIONS)

TELETYPE

KEY "CONTROL A" BEGINS DATA
 ACCUMULATION IN LOCATION A

KEY "CONTROL B" BEGINS DATA
 ACCUMULATION IN LOCATION B

KEY "A" DISPLAY A

KEY "B" DISPLAY B

KEY "S" STOP ADC

KEY "D" DISPLAY THE TWO DATA
 STORAGE LOCATIONS X AND Y
 WHERE DATA IS MOVED TO PERFORM
 VARIOUS OPERATIONS

```

DISPY: CMP TKB, #'X'      KEY "X" DISPLAY X
BNE DISPY
CLR #164002
MOV #14000, C0
MOV #400, NC
MOV #15000, LC
MOV #14000, OP0
MOV #15000, OPL
RTI

```

```

DISPY: CMP TKB, #'Y'      KEY "Y" DISPLAY Y
BNE DISPY
CLR #164002
MOV #15000, C0
MOV #400, NC
MOV #16000, LC
MOV #15000, OP0
MOV #16000, OPL
RTI

```

```

DISPW: CMP TKB, #'W'      KEY "W" DISPLAY W
BNE MOVE
CLR #164002
MOV #7000, C0
MOV #400, NC
MOV #10000, LC
MOV #7000, OP0
MOV #10000, OPL
RTI
.EOT

```

```

MOVE: CMP TKB, #'M'
BNE MOV1
MOV C0, X1
MOV #14000, X2
LP: MOV (X1)+, (X2)+
CMP X1, LC
BEQ RET
BR LP

```

KEY "M" MOVES WHATEVER IS
DISPLAYED TO X IF IT IS 256
CHANNELS; TO X AND Y (D) IF
IT IS 512 CHANNELS

```

MOV1: CMP TKB, #'I'
BNE MOV2
MOV #10000, X1
MOV #14000, X2
LR: MOV (X1)+, (X2)+
CMP X1, #11000
BEQ LR
BR LR
LR: MOV #13000, X1
MOV #15000, X2
LS: MOV (X1)+, (X2)+
CMP X1, #14000
BEQ RET
BR LS

```

KEY "SHIFT 1" SHIFTS DATA FROM
DETECTOR 1 TO LOCATION D
(DETECTOR 1 IS AT +135 DEGREES
WHEN DATA IS ACCUMULATED IN A,
BUT AT -135 DEGREES WHEN DATA
IS ACCUMULATED IN B)

```

MOV2: CMP TKB, #'2'
BNE RVRS
MOV #12000, X1
MOV #14000, X2
LT: MOV (X1)+, (X2)+

```

KEY "SHIFT 2"

```

CMP X1, #13000
BEQ LU
BR LT
LU: MOV #11000, X1
MOV #15000, X2
LV: MOV (X1)+, (X2)+
CMP X1, #12000
BEQ RET
BR LV

```

```

EVRTS: CMP TKB, #'I
BNE PLUS
MOV #14000, X1
MOV #15000, X2
LV: MOV (X1), X3
MOV -(X2), (X1)+
MOV X3, (X2)
CMP X1, #14400
BEQ LX
BR LV

```

```

LX: MOV #15000, X1
MOV #16000, X2
LY: MOV (X1), X3
MOV -(X2), (X1)+
MOV X3, (X2)
CMP X1, #15400
BEQ RET
BR LY

```

```

RET: INC KSR
RTI
PLUS: CMP TKB, #'+'
BNE MINUS
MOV #862721, OPER
RTI

```

```

MINUS: CMP TKB, #'-'
BNE NOUGHT
MOV #162721, OPER
RTI
NOUGHT: CMP TKB, #'0'
BNE WUN

```

```

MOV #1, CONST
BR BACKGR
WUN: CMP TKB, #'1'
BNE TOO
MOV #4, CONST
BR BACKGR

```

```

TOO: CMP TKB, #'2'
BNE THREE
MOV #20, CONST
BR BACKGR
THREE: CMP TKB, #'3'
BNE FOUR
MOV #100, CONST
BR BACKGR

```

KEY "I" INVERTS THE DATA IN BOTH X AND Y. (FOR TIME SPECTRA THAT HAVE BEEN COLLECTED WITH TIME REVERSED).

KEY "+" ADD BACKGROUND

KEY "-" SUBTRACT BACKGROUND (CONSTANT BACKGROUND 2 TO THE POWER 2N).

KEY "0"

KEY "1"

KEY "2"

KEY "3"


```

FOUR: CMP TKB, #'4
BNE FIVE
MOV #400, CONST
BR BACKGR
FIVE: CMP TKB, #'5
BNE SIX
MOV #2000, CONST
BR BACKGR
SIX: CMP TKB, #'6
BNE RIGHT
MOV #10000, CONST
BACKGR: MOV OP0, X1
OPER: CLR X2
CONST: CLR X2
CMP X1, OPL
BEQ RETURN
BR OPER

```

KEY "4"

KEY "5"

KEY "6"

```

RIGHT: CMP TKB, #'R
BNE LEFT
MOV OPL, X1
MOV OPL, X2
CLR -(X1)
SHIFTR: MOV -(X1), -(X2)
CMP X1, OP0
BEQ RETURN
BR SHIFTR
LEFT: CMP TKB, #'L
BNE NORM
MOV OP0, X1
MOV OP0, X2
CLR (X1)+
SHIFTL: MOV (X1)+, (X2)+
CMP X1, OPL
BEQ RETURN
BR SHIFTL

```

KEY "R" MOVES THE DATA ONE CHANNEL RIGHT

KEY "L" MOVES THE DATA ONE CHANNEL LEFT

```

.EOT
NORM: CMP TKB, #'N
BNE DIVIDE
MOV OP0, X1
NN: MOV (X1), X2
MOV #4, DN
ROT: ASR X2
BIC #100000, X2
DEC DN
TST DN
BNE ROT
ADD X2, (X1)+
CMP X1, OPL
BEQ RETURN
BR NN

```

KEY "N" TO NORMALIZE

(MULTIPLIES EVERY POINT IN THE DISPLAYED SPECTRUM BY 17/16)

```

DIVIDE: CMP TKB, #'/'
BNE ZERO
CLR X4
NUM: MOV A1(X4), X2

```

KEY "/" DIVIDES X BY Y POINT BY POINT AND STORES THE QUOTIENT IN W FOR DISPLAY

```

TST X2
BEQ Z
MOV A2(X4),X1
TST X1
BEQ Z
CLR X3
MOV #4,M
SETUP: ROR X2
ROR X3
DEC M
TST M
BIE SETUP
MOV #20,M
DIV: ASL X3
ROL X2
BEQ LUP
INC X3
SUB X1,X2
BHS LUP
ADD X1,X2
DEC X3
LUP: DEC M
TST M
BIE DIV
MOV X3,A3(X4)
COUNT: TST (X4)+
CMP X4,#A0
BIE NUM
BR A
Z: CLR A3(X4)
BR COUNT
A: CLR X4
A0=1000
A1=14000
A2=15000
A3=7000
BR RETURN
ZERO: CMP TKB,#232
BIE EXP
MOV C0,X1
AGAIN: CLR (X1)+
CMP X1,LC
BIE AGAIN
RETURN: INC KSR
RTI
TKB=177562
KSR=177560

```

KEY "CONTROL Z" ZEROS THE
DISPLAYED SPECTRUM

```

EXP: CMP TKB, #E
BVE RETURN
MOV #15000, X1
CLR: CLR (X1)+
CMP X1, #16000
BVE CLR
MOV #177570, X1
MOV #15000, X3
MOV #164006, (X3)
ASL (X3)
ASL (X3)
ASL (X3)
MOV #17, M
MOV (X3)+, X2
CLR -(X6)
CLR X4
MULT: CLC
ROR X2
ROR X4
ROL X1
TST X1
BPL BACK
ADD X2, (X3)
ADD X4, (X6)
ADC (X3)
BACK: DEC M
TST M
BVE MULT
MOV #177570, X1
MOV #17, M
MOV (X3)+, X2
MOV (X6), X4
CLR (X6)
CMP X3, #16000
BVE MULT
CLR (X6)+
RTI
.END

```

KEY "E" DEPOSITS AN EXPONENTIAL SPECTRUM IN Y

THE AMPLITUDE IS DETERMINED BY THE MARKER SWITCHES (WHICH ALSO DEFINE THE INTENSIFIED POINT)

THE RATIO OF CHANNEL N+1 TO CHANNEL N IS SET ON THE COMPUTER CONSOLE SWITCHES

REFERENCES

- Abragam A. and Pound R. V., Phys. Rev. 92, 943 (1953).
- Agarwal Y. K., Bertschat H., Haas H., Pleiter F., Recknagel E., Schlodder E. and Spellmeyer B., Phys. Lett. 47A, 161 (1974).
- Barrett J. S., Cameron J. A., Zámori Z. and Santry D. C., C.J.P. 50 #7, 619 (1972).
- Blum M., N.P. A167, 81 (1971).
- Blythe H. J., J. Phys. C1, 1604 (1968).
- Blythe H. J. and Crangle J., Phil. Mag. 18, 1143 (1968).
- Boulter J. F., Prestwich W. V and Kennett T. J., N.I.M. 27, 163 (1970).
- Cameron J. A., Campbell I. A., Compton J. P., Lines R. A. G. and Stone N. J., N.P. 52, 475 (1964).
- Cameron J. A., Gardner P. R., Prestwich W. V., Zámori Z. and Santry D. C., C.J.P. 48, 2725 (1970).
- Campbell I. A., J. Phys. C3, 2151 (1970).
- Dillenberg D. and Maris Th. A. J., Nucl. Phys. 33, 208, (1962).
- Edwards D. M. and Wohlfarth E. P., Proc. Roy. Soc. A303, 127 (1968).
- Feiock F. D. and Johnson W. R., Phys. Rev. 187, 39 (1969).
- Foner S., McNiff E. J. and Sadagopan V., Phys. Rev. Lett. 19, 1233 (1967).
- Frauenfelder H. and Steffen R. M., "Alpha, Beta and Gamma-Ray Spectroscopy V2" - K. Siegbahn, North Holland (1966).
- Frenkel J., Z. Physik 49, 31 (1928).
- Friedel J., J. Phys. Radium 19, 573 (1958), J. Phys. Radium 23, 501 (1962).
- Gabriel H., Phys. Rev. 181 #2, 506 (1969).
- Heisenberg W., Z. Physik 49, 619 (1928).

Herring C., "Magnetism", V.4, Rado and Suhl, Academic Press, New York and London (1966).

Johnson D. L., Phys. Rev. B 9 #5, 2273 (1974).

Kasuya T., Progr. Theoret. Phys. (Kyoto) 16, 45 (1956).

Keszthelyi L., Cameron J. A. and Santry D. C., C.J.P. 49 #21, 2646 (1971).

Kim D. J., Phys. Rev. B1, 3725 (1970).

Knapp G. S. and Corenzwit E., Bull. Am. Phys. Soc. 14, 348 (1969).

Knapp G. S., Fradin F. Y. and Culbert H. V., 16th Annual Conference on Magnetism and Magnetic Materials, Miami Beach (1970).

Knapp G. S., J. App. Phys. 41 #3, 1073 (1970).

Koelling D. D., Johnson D. L., Kirkpatrick S. and Mueller F. M., Sol. St. Comm. 2, 2039 (1971).

Koi Y., Tsujinura A., Tadamiki M and Kushiida K., J. Phys. Soc. Japan 16, 1040 (1961).

Low G. E. and Collins M. F., J. App. Physics 34, 1195 (1963).

Love L. M., Zmora H. and Prestwich W. V., C.J.P. 51 #14, 1497 (1973).

Matthias B. T. and Bozorth R. M., Phys. Rev. 109, 604 (1958).

Moriya T. and Kawakubo A., Tech. report of I.S.S.P. A537, (1972).

Mott N. F., Proc. Phys. Soc. (London) 47, 571 (1935).

Mott N. F., and Jones H., "The Theory of the Properties of Metals and Alloys", Oxford University Press (Clarendon), London and New York, (1936).

Murdoch B. T., Olsen C. E and Steyert W. A., Phys. Lett. 44A #6, 413 (1973).

Netz G. and Bodenstedt E., Nuc. Phys. A208, 503 (1973).

Hishihara Y., Ogawa S. and Waki S., private communication (1974).

- Oddou J. L., Berthier J., Peretto P. and Robin M., Phys. Stat. Sol. 45b, 139 (1971).
- Ogawa S., J. Phys. Soc., Japan 25, 109 (1968), Phys. Lett. 25A, 516 (1967), "Itinerant Electron Magnetism in the $ZrZn_2$ Phase", (Researches of the Electrotechnical Laboratory #735) (1972).
- Pietrokowski P., Trans. A.I.M.E., Journal of Metals, p.219 (1954).
- Rubinstein M., Strauss G. H. and Dveck J., Phys. Rev. Lett. 17, 1001 (1966).
- Ruderman M. A. and Kittel C., Phys. Rev. 96, 99 (1954).
- Schwartz B. B., "Local magnetic Moments" in "Hyperfine Interactions in Excited Nuclei V.1" (Rehovot Conference), Gordon and Breach, New York (1971).
- Shirane G., Nathans R., Pickert S. J. and Alperin H. A., International Conference of Magnetism, Nottingham, p.223 (1964).
- Shirley D. A. and Westenbarger G. A., Phys. Rev. 138 #1A 170 (1965).
- Shirley D. A., Rosenblum S. S. and Matthias E., Phys. Rev. 170 #2, 363 (1968).
- Stearns M. B., Phys. Rev. 147, 439 (1966).
- Stoner E. C., Proc. Roy. Soc. A165, 372 (1938).
- Streever R. L. and Uriano G. A., Phys. Rev. 149, 295 (1966).
- Wagner H. F. and Forker M., N.I.M. 69, 197 (1969).
- Wang S. Q., Evenson W. E. and Shrieffer J. R., Phys. Rev. Lett 23, 92 (1969).
- Wertheim G. K., Jaccarino V., Wernick J. H. and Buchanan D. N. E., Phys. Rev. Lett. 12, 24 (1964).
- Wohlfarth E. P., J. App. Phys. 39 #2, 1061 (1968).
- Yosida K., Phys. Rev. 106, 893 (1957).
- Zener C., Phys. Rev. 81, 440 (1951); Phys. Rev. 82, 403 (1951).
- Zijlstra H., "Experimental Methods in Magnetism" V.6, p.132, Wiley. New York.

PREVIOUSLY COPYRIGHTED MATERIAL, NOT FILMED.